Comparison of isoprene chemical mechanisms at atmospheric night-time conditions in chamber experiments: Evidence of hydroperoxy aldehydes and epoxy products from NO$_3$ oxidation

Philip T. M. Carlsson[1], Luc Vereecken[1], Anna Novelli[1], François Bernard[2], Steven S. Brown[3,4], Bellamy Brownwood[5], Changmin Cho[1,a], John N. Crowley[6], Patrick Dewald[6], Peter M. Edwards[7], Nils Friedrich[6], Juliane L. Fry[5,b], Mattias Hallquist[8], Luisa Hantschke[1], Thorsten Hohaus[1], Sungah Kang[1], Jonathan Liebmann[6], Alfred W. Mayhew[7], Thomas Mentel[1], David Reimer[1], Franz Rohrer[1], Justin Shenolikar[6], Ralf Tillmann[1], Epameinondas Tsiligiannis[8], Rongrong Wu[1], Andreas Wahner[1], Astrid Kiendler-Scharr[1,9,c], and Hendrik Fuchs[1,9]

[1]Institute of Energy and Climate Research, IEK-8: Troposphere, Forschungszentrum Jülich GmbH, 52428 Jülich, Germany
[2]Institut de Combustion, Aérothermique, Réactivité et Environnement (ICARE), UPR CNRS, 45071 Orléans, France
[3]NOAA Chemical Sciences Laboratory, 80309 Boulder, USA
[4]Department of Chemistry, University of Colorado, 80309 Boulder, USA
[5]Department of Chemistry, Reed College, 97202 Portland, USA
[6]Atmospheric Chemistry Department, Max Planck Institut für Chemie, 55128 Mainz, Germany
[7]Wolfson Atmospheric Chemistry Laboratories, Department of Chemistry, University of York, Heslington, York, UK
[8]Department of Chemistry and Molecular Biology, University of Gothenburg, 41296 Gothenburg, Sweden
[9]I. Physikalisches Institut, Universität zu Köln, 50932 Köln, Germany
[a]now at: School of Environmental Sciences and Environmental Engineering, Gwangju Institute of Science and Technology, Gwangju, South Korea
[b]now at: Environmental Sciences Group, Wageningen University, 6708 HB Wageningen, the Netherlands
[c]deceased

Correspondence: Philip T. M. Carlsson (p.carlsson@fz-juelich.de) and Hendrik Fuchs (h.fuchs@fz-juelich.de)

Abstract.

The gas-phase reaction of isoprene with the nitrate radical (NO$_3$) was investigated in experiments in the outdoor SAPHIR chamber at atmospherically relevant conditions specifically with respect to the chemical lifetime and fate of nitrato-organic peroxy radicals (RO$_2$). Observations of organic products were compared to concentrations expected from different chemical mechanisms: (1) The Master Chemical Mechanism, which simplifies the NO$_3$ isoprene chemistry by only considering one RO$_2$ isomer. (2) The chemical mechanism derived from experiments in the Caltech chamber, which considers different RO$_2$ isomers. (3) The FZJ-NO3 isoprene mechanism derived from quantum chemical calculations, which in addition to the Caltech mechanism includes equilibrium reactions of RO$_2$ isomers, unimolecular reactions of nitrate RO$_2$ radicals and epoxidation reactions of nitrate alkoxy radicals. Measurements using mass spectrometer instruments give evidence that the new reactions pathways predicted by quantum chemical calculations play a role in the NO$_3$ oxidation of isoprene. Hydroperoxy aldehydes (HPALD), which are specific for unimolecular reactions of nitrate RO$_2$, were detected even in the presence of an OH scavenger excluding the possibility that concurrent oxidation by hydroxyl radicals (OH) is responsible for their formation. In addition, ion signals at masses that can be attributed to epoxy compounds, which are specific for the epoxidation reaction of

nitrate alkoxy radicals, were detected. Measurements of methyl vinyl ketone (MVK) and methacrolein (MACR) concentrations confirm that the decomposition of nitrate alkoxy radicals implemented in the Caltech mechanism cannot compete with the ring-closure reactions predicted by quantum-chemical calculations. The validity of the FZJ-NO3 isoprene mechanism is further supported by a good agreement between measured and simulated hydroxyl radical (OH) reactivity. Nevertheless, the FZJ-NO3 isoprene mechanism needs further investigations with respect to the absolute importance of unimolecular reactions of nitrate RO_2 and epoxidation reactions of nitrate alkoxy radicals. Absolute concentrations of specific organic nitrates such as nitrate hydroperoxides would be required to experimentally determine product yields and branching ratios of reactions but could not be measured in the chamber experiments due to the lack of calibration standards for these compounds. The temporal evolution of mass traces attributed to products species such as nitrate hydroperoxides, nitrate carbonyl, nitrate alcohols as well as hydroperoxy aldehydes observed by the mass spectrometer instruments demonstrates that further oxidation by the nitrate radical and ozone at atmospheric concentrations is small on the time scale of one night (12 hours) for typical oxidant concentrations. However, oxidation by hydroxyl radicals present at night and potentially also produced from the decomposition of nitrate alkoxy radicals can contribute to their nocturnal chemical loss.

1 Introduction

Isoprene (C_5H_8) is an unsaturated compound and the most emitted non-methane hydrocarbon in the atmosphere. Circa $500\,Tg$ per year of isoprene is emitted by plants as co-product of photosynthesis activity (Guenther et al., 2012). The high reactivity of isoprene towards the most important daytime oxidant, the hydroxyl radical (OH), results in a chemical lifetime of a few hours for typical atmospheric conditions, so that the majority of isoprene is oxidized during the day. However, isoprene can also be present in significant quantities after sunset, when the production rate of OH radicals is low, so that oxidation by the nitrate radical (NO_3) or ozone can gain in importance (Brown et al., 2009; Edwards et al., 2017).

Oxidants add preferentially to the C=C double bonds in isoprene initiating a cascade of radical reactions. Theoretical studies of the OH-initiated oxidation of isoprene showed that the primary organic peroxy radicals (RO_2) formed after the OH addition are in a thermal equilibrium with the alkyl radical through oxygen elimination and re-addition reactions at a time scale that is short relative to the chemical lifetimes of the RO_2 radicals at atmospheric conditions (Peeters et al., 2009, 2014). As a consequence, fast H-shift reactions of RO_2 isomers can constitute a large loss process for the entire RO_2 pool. This applies to the 1,6-H-migration reactions of the Z-δ-RO_2 isomers produced from the isoprene + OH reaction (Peeters et al., 2014). These H-migrations lead eventually to the regeneration of OH radicals. Because this type of radical regeneration does not require the presence of nitric oxide (NO), it can significantly enhance radical concentrations in forested environments (Novelli et al., 2020). The OH initiated oxidation of isoprene has been investigated in laboratory (Crounse et al., 2011; Berndt et al., 2019) and simulation chamber studies (Fuchs et al., 2013; Novelli et al., 2020), which contributed to the refinement of the chemical mechanism proposed by the theoretical studies. The results can partly explain high OH radical concentrations observed in field experiments in rainforests (Lelieveld et al., 2008; Whalley et al., 2011).

In contrast to daytime, the loss of RO_2 radicals due to the reaction with NO does not play a role at night in the absence of near emission sources because NO production from the photolysis of NO_2 is stopped and NO is rapidly titrated to NO_2 by the reaction with ozone. In some situations, ozone can also be locally completely consumed in the night if there are high NO emissions for example from traffic or from power plants. In this case, NO can accumulate. However, for these conditions, the nitrate radical is rapidly lost in the reaction with NO. Therefore, it is unlikely that nitrate RO_2 radicals and NO exist simultaneously. Thus, nitrate RO_2 from the reaction of NO_3 with organic compounds are expected to react mainly with hydroperoxy radicals (HO_2), other organic peroxy radicals, the nitrate radical or they may undergo unimolecular reactions.

In previous chamber and laboratory studies investigating the reaction of isoprene with NO_3, the fate of RO_2 was often dominated by RO_2 self- and cross-reactions and RO_2 reactions with NO_3 due to high reactant concentrations (Barnes et al., 1990; Kwok et al., 1996; Perring et al., 2009; Kwan et al., 2012). A chamber study by Schwantes et al. (2015) focussed on the product distribution from the reaction of nitrate RO_2 with HO_2 because this reaction pathway is generally the dominant loss path in the atmosphere. Chamber studies by Rollins et al. (2009) and Ng et al. (2008) were also designed to reproduce atmospheric chemical conditions, for which the nitrate RO_2 reacts in various pathways.

Near-explicit chemical mechanisms such as the Master Chemical Mechanism (Jenkin et al., 2015) and the isoprene mechanism developed by Wennberg et al. (2018) (called Caltech mechanism in this work) were partly built by using results from

these studies. In addition, it has been proposed that the nitrate RO_2 radicals formed from the reaction of the nitrate radical with isoprene can interconvert at ambient temperature (Wennberg et al., 2018; Vereecken et al., 2021). This can enhance the importance of unimolecular reactions of specific RO_2 if the chemical lifetime of the RO_2 radicals is long enough that concentrations can re-equilibrate.

65   Furthermore, the theoretical study by Vereecken et al. (2021) revealed that unimolecular reactions of alkoxy radicals formed in the radical reaction chain subsequent to the addition of NO_3 to isoprene lead to the production of epoxide RO_2, influencing the distribution of organic products. This newly identified chemistry is included only in the FZJ-NO3 isoprene mechanism published by Vereecken et al. (2021).

The aim of this study is to compare the NO_3 isoprene chemistry of different available explicit mechanisms (MCM, Caltech
70   and FZJ-NO3) with respect to the fate of nitrato-organic peroxy radicals and the distribution of organic products for a series of chamber experiments performed at atmospherically relevant night-time conditions.

2   Methods

2.1   Experiments in the SAPHIR chamber

The experiments discussed in this work were performed in the atmospheric simulation chamber SAPHIR (Rohrer et al., 2005)
75   at Forschungszentrum Jülich in 2018. The chamber is a 270 m^3 double-wall reactor. It is operated at a slight overpressure of 35 Pa to prevent ambient air from leaking into the chamber. The space between the 2 films is continuously flushed with pure nitrogen to prevent contamination of the inner chamber. The walls are made of Teflon film (FEP) and are thus chemically inert while the full solar spectrum is transmitted into the chamber (Bohn and Zilken, 2005). Night-time can be simulated by a shutter system that covers the chamber. Synthetic air used for flushing the chamber and for replenishing losses due to
80   sampling of instruments and leakage is produced from evaporating and mixing high purity liquid nitrogen and oxygen (purity: 99.9999 %, Linde). Inside the chamber, 2 fans are operated to ensure homogeneous mixing of air. The temperature inside the chamber is similar to ambient temperature and ranged between 291 and 308 K with maximum values in the afternoon for the experiments in this work.

Reactive trace gases added to the chamber in the experiments were ozone produced by a silent discharge ozonizer (O3onia),
85   isoprene (C_5H_8, purity: 99 %, Sigma Aldrich), propene (purity: 99.8 %, Linde), CO (purity: 99.997 %, Linde) and NO_2 (purity: 99.2 %, 519 ppmv in nitrogen, Linde). Addition of gaseous species were controlled by calibrated mass flow controllers. Isoprene was injected as a liquid with a syringe into a hot volume and the vapour was flushed into the chamber together with the replenishment flow of zero air.

Four experiments performed on 09, 10, 12, and 13 August 2018 (Experiment #1, #2, #3, #4) are analysed in this work
90   (Table 1, Fig. 1, 2, A1, A2). Before each experiment, the chamber was flushed overnight with a high flow of zero air, so that concentrations of trace gases from previous experiments were below the limit of detection of instruments. The chamber roof was always closed to simulate night-time conditions. Experiments were performed in dry synthetic air. NO_3 was produced by the reaction of NO_2 and O_3. Typical mixing ratios after the injection were 5 ppbv NO_2 and 100 ppbv O_3. NO_3 production
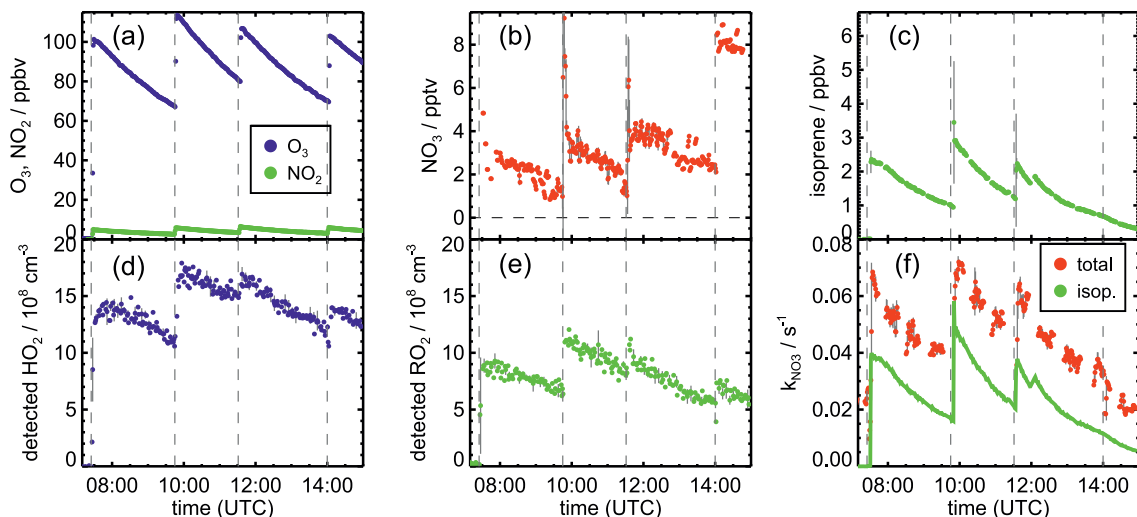
Figure 1. Measurements of radical and trace gas concentrations and NO_3 reactivity in the experiment on 09 August 2018 (Experiment #1) investigating the oxidation of isoprene by NO_3. Between 100 and 200 ppmv propene was present to produce HO_2 radicals by its ozonolysis. OH radicals, which are produced in the ozonolysis reaction, are rapidly converted to HO_2 in the reaction with 70 to 120 ppmv CO that was injected at the start of the experiment. OH reactivity was dominated by the high CO concentration and is not shown. NO_3 reactivity does not include reactivity from organic radicals and NO_2. NO_3 reactivity from isoprene is calculated from measured isoprene concentrations and reaction rate constants recommended in the literature (Mellouki et al., 2021). The difference between measured reactivity and reactivity from isoprene can be attributed to propene in this experiment. Observed RO_2 radicals only include a fraction of the total RO_2 because the LIF instrument cannot detect all RO_2 species formed in the reaction of isoprene with NO_3 (Vereecken et al., 2021).

rates ranged between 0.9 and 11 ppbv/hour. Highest NO_3 production rates were reached in the experiment on 13 August 2018
95 (Experiment #4) and lowest rates in the experiment on 10 August 2018 (Experiment #2).

After NO_3 production started, isoprene was added. The injection of all three species was repeated after a few hours, when most of the isoprene had been consumed. Only NO_2 and O_3 were re-injected to enhance NO_3 production in the last part of the experiments, except for the experiment on 10 August 2018 (Experiment #2). In the experiment on 09 August 2018 (Experiment #1), propene was injected to enhance HO_2 concentrations by radical production via its ozonolysis. Excess CO was additionally
100 injected to convert OH radicals to HO_2.

In the experiments in this work, no measurable secondary organic aerosol was formed, so that loss of products species on aerosol did not play a role (Brownwood et al., 2021).

The total amount of isoprene that was consumed by NO_3 was (3.2 ± 0.5) ppbv, (2.5 ± 0.5) ppbv, (4.8 ± 0.5) ppbv, and (11.6 ± 1.2) ppbv in the in the experiments on 09, 10, 12, and 13 August 2018 (Experiment #1, #2, #3, #4), respectively
105 (Brownwood et al., 2021). Approximately 10 % of the total isoprene consumed in the experiment reacted with ozone except for the experiment on 09 August 2018 (Experiment #1), when 25 to 30 % of isoprene was lost in the reaction with ozone due to the low NO_3 and high ozone concentration. In addition, measurements of OH radicals suggest that up to 10 % of isoprene
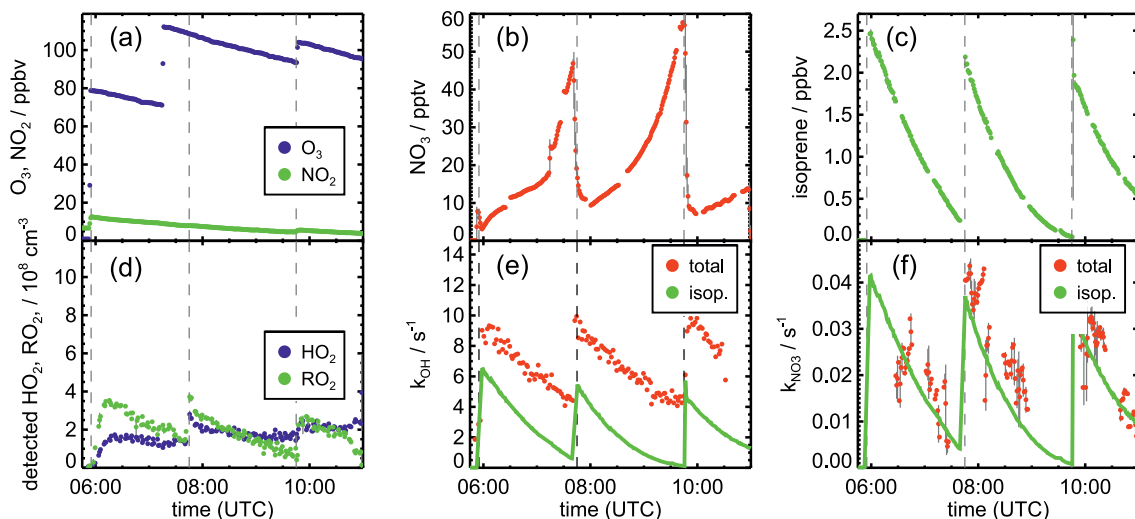
Figure 2. Measurements of radical and trace gas concentrations and OH and NO_3 reactivity in the experiment on 13 August 2018 (Experiment #4) investigating the oxidation of isoprene by NO_3, when the total amount of oxidized isoprene was highest. OH and NO_3 reactivity from isoprene is calculated from measured isoprene concentrations and reaction rate constants recommended in the literature (Mellouki et al., 2021). NO_3 reactivity does not include reactivity from organic radicals and NO_2. Observed RO_2 radicals only include a fraction of the total RO_2 because the LIF instrument cannot detect all RO_2 species formed in the reaction of isoprene with NO_3 (Vereecken et al., 2021).

reacted with OH in the experiments without OH scavenger. However, OH concentration measurements were close to the limit of detection of the instrument, so that the fraction of isoprene that reacted with OH is rather uncertain. Overall, the dominant

110 loss for isoprene was due to the reaction with NO_3 radicals (80 to 90 % of the total loss in most of the experiments).

The chemical conditions in the experiments were chosen such that the chemical loss of nitrated RO_2 radicals differed between the experiments (Table 1). Similar as for typical night-time conditions in the nocturnal residual layer in the absence of nearby sources, nitric oxide concentrations were zero, so that RO_2 reacted only with either HO_2, RO_2 or NO_3 or re-arranged in unimolecular RO_2 reactions (Vereecken et al., 2021).

115 In the experiments, the concentrations of NO_3 precursor species, HO_2, O_3 and NO_2, and of isoprene were varied. As a consequence, RO_2 concentrations differed between these experiments and therefore also the relative importance of RO_2 loss reactions.

2.2 Instrumentation

A large suite of instruments detected inorganic and organic species during the experiments. Isoprene and its oxidation products
120 were measured by a proton transfer reaction time-of-flight mass spectrometer (VOCUS PTR-MS, Aerodyne, Krechmer et al. (2018)). The instrument was calibrated for isoprene, methyl vinyl ketone and methacrolein. The sensitivity of the instrument for isoprene was higher by a factor of 1.4 in dry air than in humid air in which calibration measurements were performed

(Brownwood et al., 2021). Measured concentrations were corrected for this humidity effect. No calibration standards were available for organic nitrate products such as nitrated alcohols, carbonyls, hydroperoxides and epoxides.

125   Organic compounds were also detected by 2 other chemical ionization mass spectrometer instruments (CIMS) that used either Br^- (Albrecht et al., 2019; Wu et al., 2021) or I^- as reagent ions (Tsiligiannis et al., 2022). These instruments detected various oxygenated organic product species, but were not calibrated to provide concentrations. Details of the measurements by the Br^- CIMS instrument can be found in Wu et al. (2021) and by the I^- CIMS instrument in Tsiligiannis et al. (2022).

    The high resolution of the mass spectrometer instruments allowed to attribute the ion mass signals (m/z) to sum formulas

130 of organic compounds (Table A1). In this work, ion signals that were highest among all signals are discussed, most of which can be attributed to products of the isoprene oxidation (Wu et al., 2021; Tsiligiannis et al., 2022). Compared to the CIMS instruments, the precision of measurements by the VOCUS PTR-MS instrument was higher for organic compounds that contain few oxygens. In general, the sensitivity of CIMS instruments can be different for different isomers and functional groups, so that a change in the distribution of isomers could partly explain observed differences between instruments (Lee et al., 2014a;

135 Xiong et al., 2015, 2016). In addition, changes in the operational conditions of the instrument such as the temperature of the ionization region can lead to a variability of the instrument's sensitivity (Robinson et al., 2022).

    The total organic nitrate concentration was measured by 2 instruments, in which the total NO_2 concentration was detected either by a custom-built (Sobanski et al., 2016) or commercial cavity ring-down instrument (Keehan et al., 2020) after thermal dissociation of nitrate compounds in a heated inlet (TD-CRDS). A common data set from both instruments was created for this

140 campaign. Details of these measurements can be found in Brownwood et al. (2021). These instruments also measured NO_2 in the sampled air in a separate mode or second measurement channel. In addition, NO_2 concentrations were measured by another custom-built cavity ring-down instrument (Liebmann et al., 2018) and a commercial chemiluminescence instrument combined with a blue-light converter (Eco-Physics). NO_2 concentration measurements from all instruments were combined to one common, quality-checked data set (Brownwood et al., 2021). Ozone concentrations were measured by a commercial

145 instrument using UV-absorption (Ansyco).

    NO_3 and N_2O_5 concentrations were measured with 2 custom-built instruments applying cavity-ring-down spectroscopy (Wagner et al., 2011; Sobanski et al., 2016). NO_3 was detected at 662 nm and the sum of NO_3 and N_2O_5 in a second channel, in which the inlet and cavity is heated to thermally decompose N_2O_5. Measurements were combined to one data set taking also into account that NO_3 and N_2O_5 can be expected to be in a thermal equilibrium for conditions of the experiments in this

150 work.

    HO_2, OH and RO_2 radical concentrations were determined by a laser-induced fluorescence instrument (Fuchs et al., 2011, 2012; Cho et al., 2021). OH radicals are excited at 308 nm in a low-pressure cell and their fluorescence is measured by gated single-photon counting. The fluorescence cell for the detection of only OH radicals was equipped with a chemical modulation reactor (CMR), which allows to account for potential interferences in the measurements (Cho et al., 2021). In

155 another fluorescence cell, HO_2 radicals are chemically converted to OH in their reaction with NO. RO_2 radicals are converted eventually to OH in a third measurement channel (ROxLIF) that consists of an RO_2 converter, in which RO_2 and OH radicals are firstly converted to HO_2 in the presence of NO and CO, and a fluorescence cell downstream of the converter, in which the

Table 1. Chemical conditions in the experiments in this work. Experiments analysed in this work were performed in dry air. Mixing ratios of trace gases give the range of values reached right after their injection.

	Experiment #1 09 August 2018	Experiment #2 10 August 2018	Experiment #3 12 August 2018	Experiment #4 13 August 2018
O_3 / ppbv	70–120	40–70	70–110	75–110
NO_2 / ppbv	2–6	3–5	4–12	10–25
isoprene /ppbv	1–2.5	0.5–2	0.3–3	0–8
propene / ppbv	100–200	0	0	0
CO / ppmv	70–120	<0.1	<0.1	<0.1
NO_3 / pptv	1–10	5–40	5–60	10–500
T / K	295–299	292–300	288–308	291–298
data reference	Fuchs et al. (2018a)	Fuchs et al. (2018b)	Fuchs et al. (2018c)	Fuchs et al. (2018d)

sum of all radicals is detected by OH fluorescence after HO_2 has reacted with excess NO. Recent studies confirmed that not all nitrate RO_2 radicals can be detected by the ROxLIF method as they do not form HO_2 or OH radicals after reacting with NO (Ashbourn et al., 1998; Novelli et al., 2021; Vereecken et al., 2021).

OH reactivity (k_{OH}, the inverse of the chemical lifetime of the OH radical) was determined by a laser flash photolysis instrument, in which the time resolved decay of artificially produced OH radicals is observed (Fuchs et al., 2017). If, as in this work, the OH-reactivity from inorganic compounds is known, the contribution from organic compounds can be derived and compared to values based on the measurements of single compounds (Tan et al., 2021; Hantschke et al., 2021). In general, differences between measured and calculated OH reactivity can be used to determine if the detection of organic products that are reactive towards OH are complete.

The NO_3 reactivity was also measured in this work (Liebmann et al., 2017; Dewald et al., 2020). The concentration of artificially produced NO_3 is measured by cavity ring-down spectroscopy after reaction with either ambient or zero air in a flow tube. The NO_3 reactivity can be then calculated from the relative change of NO_3 concentrations between the two modes. In order to obtain the NO_3 reactivity from organic compounds, the contribution of NO_2 and NO_3 losses in the flow tube were accounted for. NO_3 reactivity from HO_2 and RO_2 radicals is not detected by the instrument due to loss of radicals in the inlet system (Dewald et al., 2020).

2.3 Modelling of trace gas concentrations

Trace gas concentrations were calculated using a chemical box model. In this work, three near-explicit chemical models have been applied: (1) The Master Chemical Mechanism version 3.3.1 (MCM) (Jenkin et al., 1997; Saunders et al., 2003; Jenkin et al., 2015), (2) the isoprene oxidation mechanism as introduced in the review article by Wennberg et al. (2018) and available

at Bates and Wennberg (2017) (Caltech), and (3) the NO_3 isoprene mechanism based on theoretical calculations by Vereecken et al. (2021) and detailed in the supplement of Vereecken et al. (2021) (FZJ-NO3 mechanism).

The Caltech mechanism includes reactions of isoprene and isoprene product species but does not include further reactions of organic products that are not specific products from the oxidation of isoprene such as glyoxal or methyl glyoxal. In this work, the Caltech mechanism is therefore extended with chemistry from the MCM for those species.

The FZJ-NO3 mechanism only includes the reaction steps subsequent to the initial addition of NO_3 to isoprene, but the chemistry of organic products was not investigated in Vereecken et al. (2021). The chemistry of the trace gases not considered in Vereecken et al. (2021) is taken from the Caltech mechanism. The isoprene OH oxidation scheme is applied as described in the work by Novelli et al. (2020), where the OH oxidation of isoprene was investigated in chamber experiments. Further chemistry of organic products that are not specific for the oxidation of isoprene are taken from the MCM. Chemical loss of first-generation organic products which are not included in either the Caltech or the MCM models is estimated from similarities to other organic products.

In the model runs, the injections of trace gases in the experiments were implemented as source reactions, which are effective during the short period of time during the injection. The rates are adjusted, such that the concentration change of the injected trace gas matches the observed increase in the concentration at the time of the injection. Physical parameters such as temperature and pressure were constrained to measured values. NO_3 was also constrained to measured values, in order to decouple its modelled concentrations from wall reactions of NO_3 and N_2O_5, which are dependent on the chemical conditions of the experiment and hence hard to characterize accurately (Dewald et al., 2020). With NO_3 concentrations constrained to measurements, the measured decay of isoprene, which is dominated by the reaction with NO_3 for most of the time, is well described by the model, confirming that measured NO_3 concentrations are consistent with the chemical loss of isoprene.

3 NO_3 oxidation mechanisms of isoprene

The initial reaction steps in the oxidation of isoprene by NO_3 (Vereecken et al., 2021) are similar to the oxidation by OH. H-atom abstraction from isoprene by NO_3 is estimated to be at least 2 orders of magnitude slower than NO_3 addition, based on the available literature data on aliphatic and allylic H-abstraction reactions (Canosa-Mas et al., 1991; Atkinson et al., 2006) and therefore not further considered in this work.

NO_3 adds to either of the C=C double bonds leading to allyl-resonance stabilized alkyl radicals. Reversible oxygen addition and elimination reactions produce 3 different RO_2 stereoisomers each from the addition of NO_3 on carbon C_1 and C_4 (Fig. 3). The different RO_2 isomers rapidly reach equilibrium concentrations. NO_3 adds preferably on carbon C_1 (yield of 87 %). The yield is higher in comparison to the corresponding OH addition (yield of 61 %). The additions on the inner carbons (C_2 and C_3) are expected to be of minor importance (Vereecken et al., 2021) and are not further considered in this work.

The isoprene NO_3 mechanisms investigated in this work differ significantly in the treatment of the initially formed RO_2. The FZJ-NO3 mechanism includes 6 RO_2 isomers formed subsequently to the NO_3 addition (Fig. 3). Specifically, the Z- and E-RO_2 isomers of the δ-RO_2 isomers are distinguished. In contrast, the Caltech mechanisms only treats δ- and β-RO_2 isomers
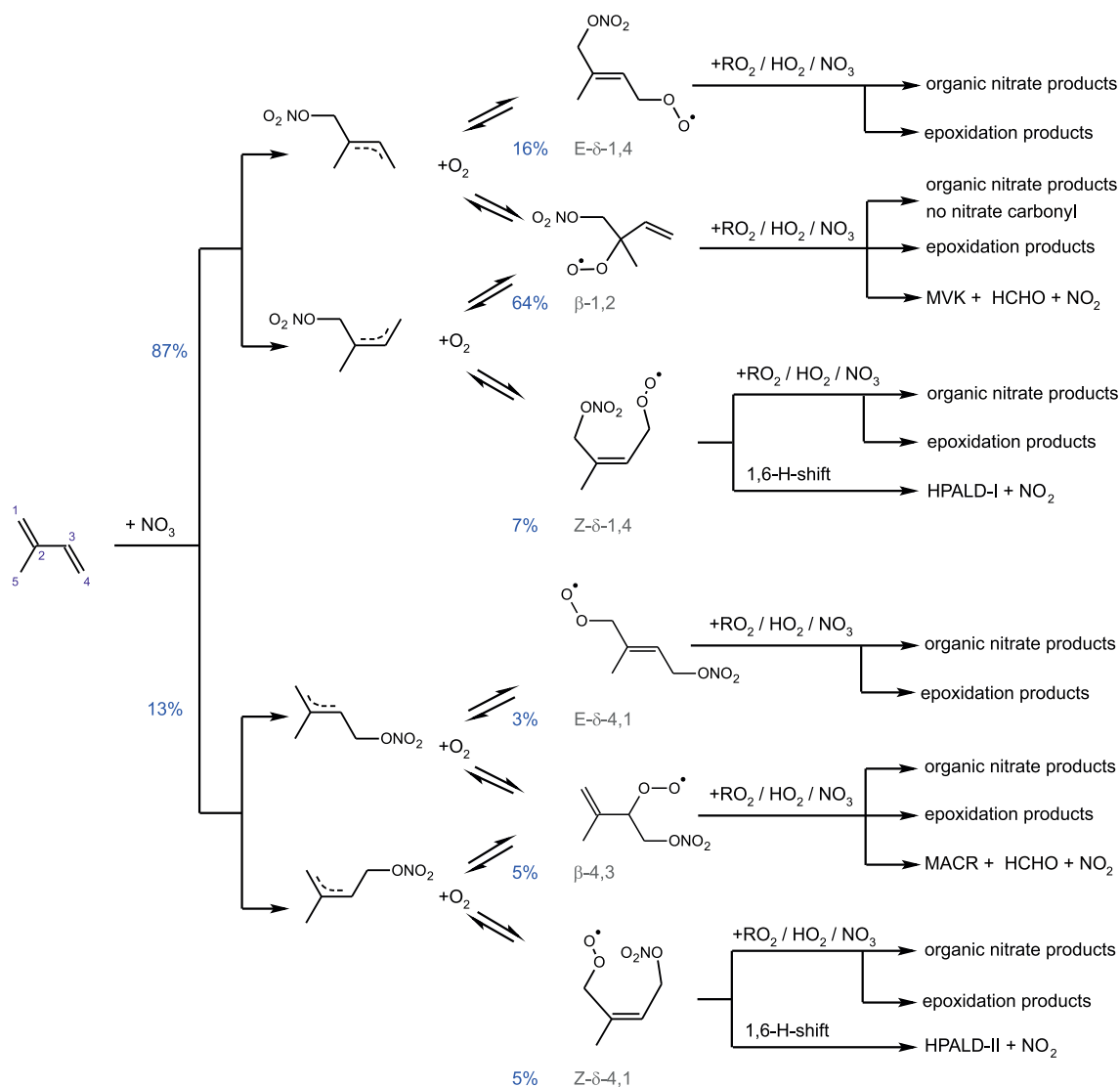
Figure 3. Schematic reaction mechanism of the reaction of isoprene with NO_3 as described in Vereecken et al. (2021). This includes fast inter-conversion of nitrate RO_2 isomers by oxygen addition and elimination reactions. Only RO_2 isomerization reactions (Vereecken et al., 2021) which can compete with bimolecular reactions for typical night-time conditions are shown. Percentage values given next to the structure of RO_2 radicals are yields when equilibrium concentrations are established for typical night-time conditions such as in the experiments in this work.

210   separately but does not include the equilibrium reactions between RO_2 isomers. The MCM simplifies the addition of NO_3 to isoprene even more by only considering the addition of NO_3 on carbon C_1 leading to the δ-RO_2 radical.

    It is important to distinguish between Z- and E-RO_2 isomers because isomer-specific unimolecular H-shift reactions need to be considered. Competitive unimolecular H-shift-reactions only occur for the Z-δ-RO_2 (Vereecken et al., 2021) leading to the formation of hydroperoxy aldehydes (HPALD) (Fig. 3). Due to the re-equilibration reactions between RO_2 isomers, these

215   reaction channels can gain in importance if the rate of this RO_2 loss reaction (0.01 to $0.05\,s^{-1}$) is faster than the chemical loss due to bimolecular RO_2 reactions. This will often be the case for night-time conditions, when mainly slow bimolecular RO_2 reactions with NO_3, HO_2 and other RO_2 radicals occur.

    The distribution of organic products from the NO_3 oxidation of isoprene depends highly on the competition between the different RO_2 loss reactions. The bimolecular reaction of nitrate RO_2 with HO_2 radicals leads to the formation of nitrate

220   hydroperoxides (NISOPOOH). Whereas one NISOPOOH isomer is the exclusive product of the RO_2+HO_2 reaction in the MCM, the Caltech and FZJ-NO3 mechanisms include not only different isomers but also the decomposition of the initially formed HO_2-RO_2 reaction complex into an OH radical and a nitrate alkoxy radical with a yield of approximately $50\,\%$ for nitrate β-RO_2 radicals.

    Nitrate alkoxy radicals can also be the product of RO_2+RO_2 reactions, but this reaction channel competes with the pro-

225   duction of nitrate carbonyls (NC_4CHO) and nitrate alcohols ($ISOPCNO_3$). Alkoxy radicals are additionally formed from the reaction of nitrate RO_2 with NO_3 accompanied by the production of NO_2. The nitrate alkoxy radicals are expected to rapidly decompose (Novelli et al., 2021; Vereecken et al., 2021). In the MCM, the decomposition leads exclusively to the formation of one isomer of the nitrate carbonyl product (NC_4CHO) together with an HO_2 radical. A similar mechanism is implemented in the Caltech and FZJ-NO3 mechanisms for most of the various nitrate alkoxy radical species except for those radicals produced

230   from the most abundant β-1,2-RO_2 isomer, from which nitrate carbonyl species cannot be formed.

    The yield of ROOR compounds from the gas-phase reaction of RO_2+RO_2 radicals is expected to be small. Due to their low volatility, however, ROOR compounds are important for the formation of SOA (Ng et al., 2008).

    In the Caltech mechanism, decomposition of these nitrate alkoxy radicals leads instantly to the formation of methyl vinyl ketone (MVK) or methacrolein (MACR) together with formaldehyde and NO_2. This was determined from chamber experi-

235   ments reported in Schwantes et al. (2015), in which a high yield of MVK was found, when nitrate RO_2 mainly reacted with HO_2. The fate of nitrate alkoxy radicals was also investigated by Vereecken et al. (2021). Quantum chemical calculations show that the decomposition reaction is slower than the ring-closure reactions leading to epoxide products. In contrast, 4-membered ring closure (barrier $\sim 25\,kcal/mol$, Vereecken (2022)) requires breaking the planar double bond to bring the radical O-atom in an appropriate position for bonding. 5- to 6-membered ring closure (barrier $\sim$ 13-29 $kcal/mol$, Vereecken et al. (2021)) are

240   also favourable.

    Differences between the chemical mechanisms also exist concerning the type of chemical loss reactions of first-generation stable organic products. Reactions with OH are considered in all mechanisms applying similar reaction rate constants. In addition, the MCM includes loss of isoprene organic nitrates due to ozonolysis reactions.
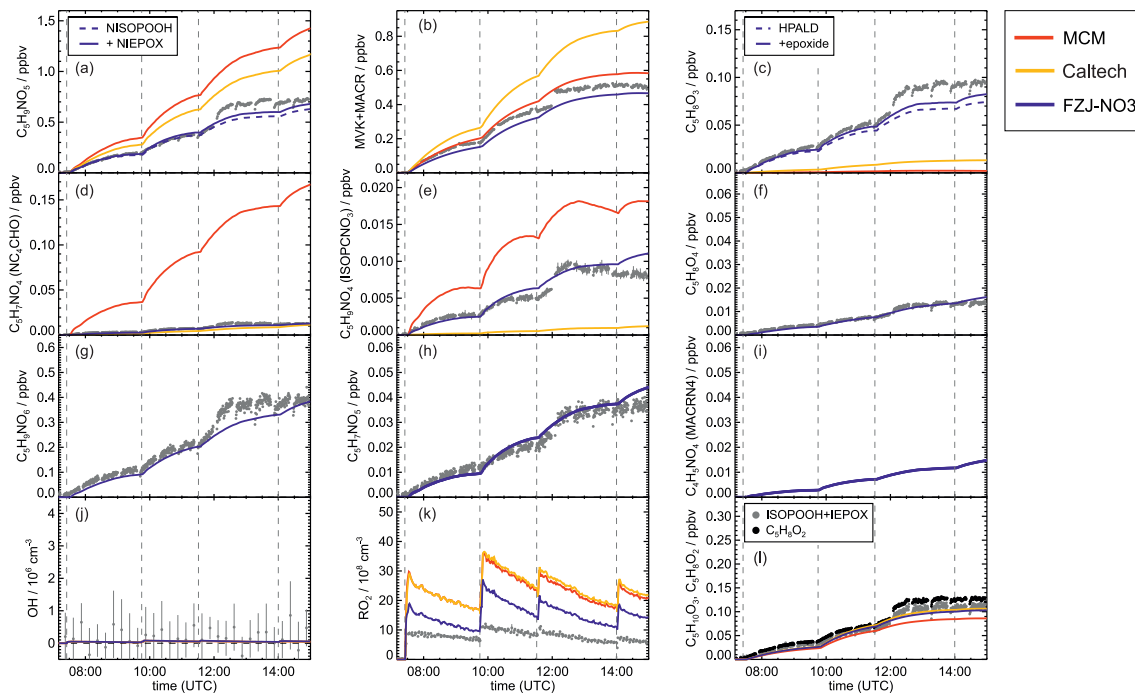
Figure 4. Comparison of results from model calculations applying the different isoprene NO_3 chemistry mechanisms for the experiment on 09 August 2018 (Experiment #1), when HO_2 concentrations were enhanced and excess CO was present as OH scavenger. MVK, MACR, NISOPOOH, $ISOPCNO_3$ and NC_4CHO are produced from all mechanisms, whereas the other species are only produced from either 1,6-H-shift reactions or ring-closure reactions of nitrate alkoxy radicals only implemented in the FZJ-NO3 mechanism. Grey and black dots are measured values. Measured organic peroxy radical concentrations only include part of the total RO_2 because the LIF instrument cannot detect a fraction of nitrate RO_2 (Vereecken et al., 2021). Organic products were detected by the VOCUS PTR-MS instrument, which was only calibrated for MVK and MACR. All other traces are scaled to match best the results from the FZJ-NO3 mechanism.

4 Results

245 Results of the model calculations are shown in Fig. 4 for the experiment on 09 August 2018 (Experiment #1), when high HO_2 concentrations were present, and therefore the main loss path for RO_2 was the reaction with HO_2. Figure 5 shows results for the experiment on 13 August 2018 (Experiment #4), when RO_2 loss was distributed among all pathways that are relevant during night-time (Brownwood et al., 2021) and the amount of oxidized isoprene was highest. Results from the other experiments are shown in the Appendix (Fig. A5, A6). In all figures, ion mass signals of the VOCUS PTR-MS instrument for which no

250 calibration was available were scaled to concentrations predicted by the FZJ-NO3 model.

Highest HO_2 concentrations of up to $17 \times 10^8 \, \mathrm{cm^{-3}}$ were measured in the experiment on 09 August 2018 (Experiment #1), when HO_2 was enhanced by production of OH radicals in the ozonolysis of propene, which were rapidly converted to HO_2 in the presence of excess CO (Fig. 1, Panel (d)). In the other experiments, measured HO_2 concentrations were between
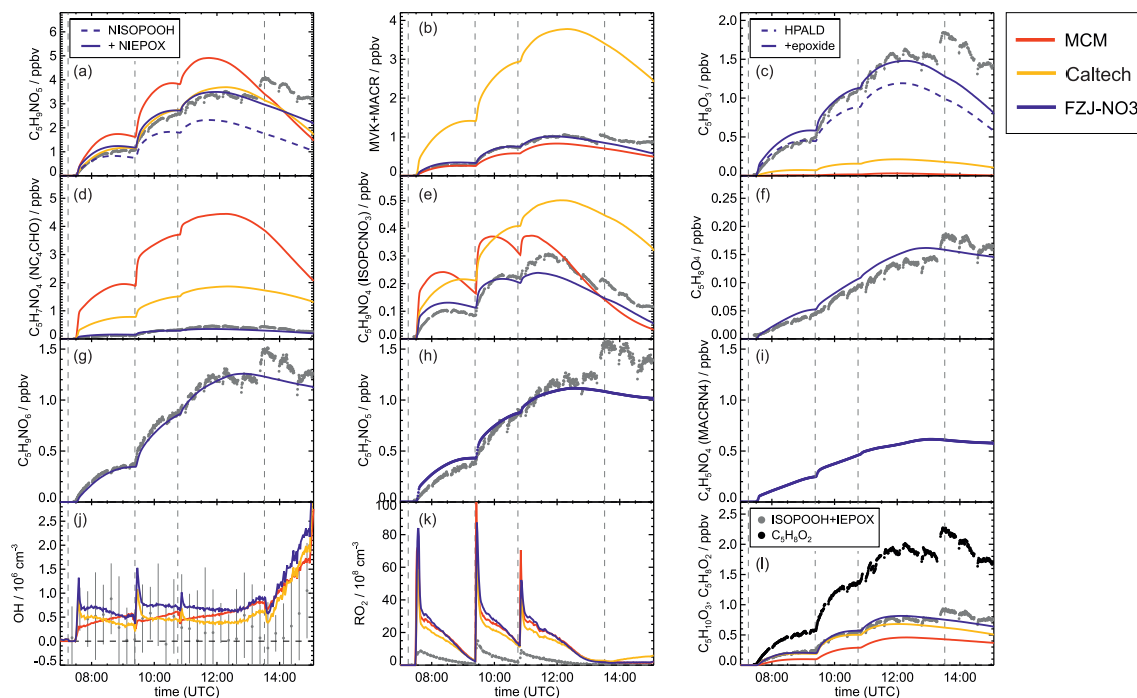
Figure 5. Comparison of results from model calculations applying the different isoprene NO_3 chemistry mechanisms for the experiment on 13 August 2018 (Experiment #4), when the amount of oxidized isoprene was highest. MVK, MACR, NISOPOOH, $ISOPCNO_3$ and NC_4CHO are produced from all mechanisms, whereas the other species are only produced from either 1,6-H-shift reactions or ring-closure reactions of nitrate alkoxy radicals only implemented in the FZJ-NO3 mechanism. Grey and black dots are measured values. Measured organic peroxy radical concentrations only include part of the total RO_2 because the LIF instrument cannot detect a fraction of nitrate RO_2 (Vereecken et al., 2021). Organic products were detected by the VOCUS PTR-MS instrument, which was only calibrated for MVK and MACR. All other traces are scaled to match best the results from the FZJ-NO3 mechanism.

1 and $5 \times 10^8 \, \text{cm}^{-3}$ with highest values in the experiment on 13 August 2018 (Experiment #4). As discussed in Vereecken et al. (2021), the measured HO_2 concentrations are much higher than predicted by model calculations for experiments in this work (up to a factor of 10) except for the experiment on 09 August 2018 (Experiment #1). Although it is possible that part of the measured HO_2 radicals is due to an interference (Vereecken et al., 2021), the HO_2 radical concentrations predicted by the model are too low to explain observed OH radical concentrations for example during the last part of the experiment on 13 August 2018 (Experiment #4) (Section 5.5). Therefore, the measured HO_2 radical concentrations are used in the further analysis in this work.

A large fraction of nitrate RO_2 radicals cannot be detected by the LIF instrument used in this work (Novelli et al., 2021; Vereecken et al., 2021) because the detection scheme of the instruments requires that HO_2 or OH radicals are formed subsequent to the reaction of RO_2 with NO. However, this is only the case for some of the nitrate RO_2 radicals from the reaction of
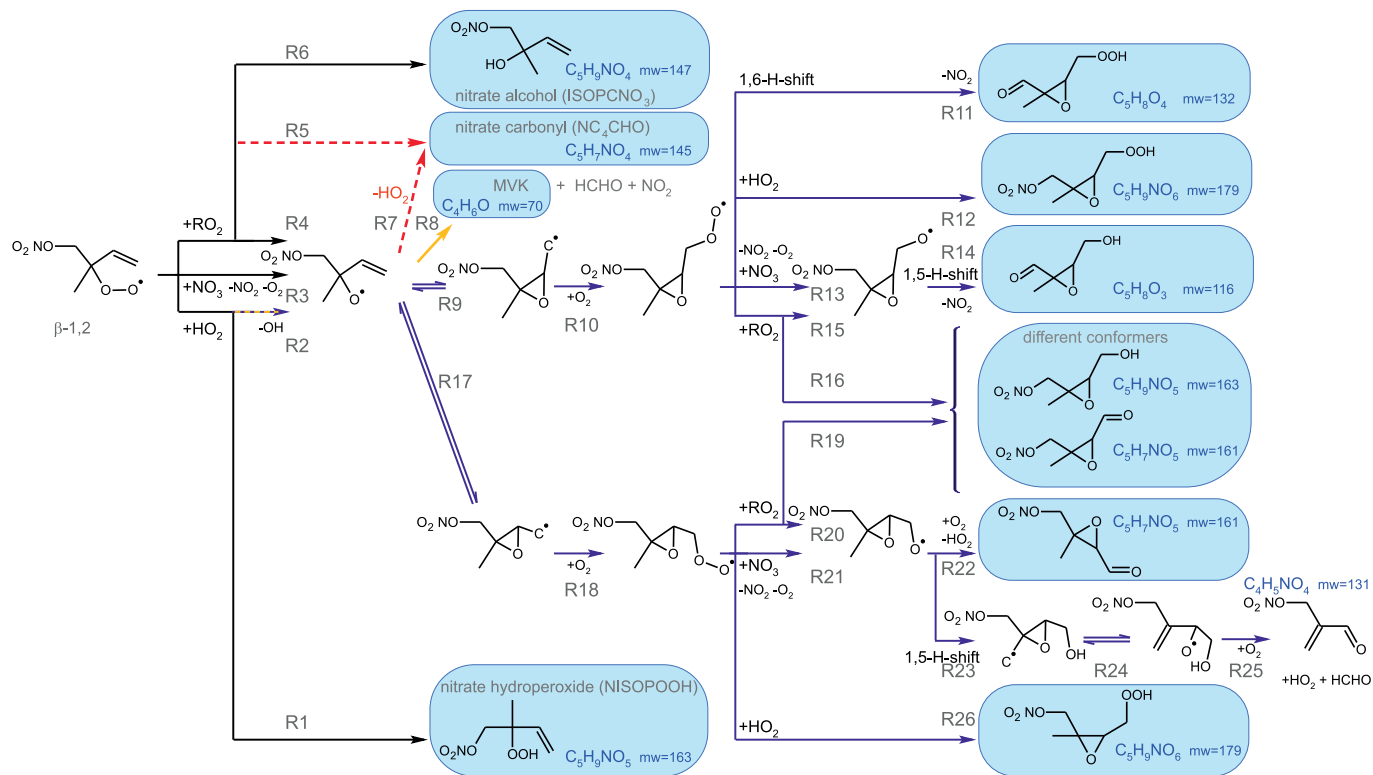
Figure 6. Loss reactions of the most abundant β-1,2-RO$_2$ species. Coloured arrows indicate the preferred reaction channel for the nitrate alkoxy radical in the different chemical models (yellow: Caltech; blue: FZJ-NO3). Dashed red arrows indicate corresponding reactions of the δ-RO$_2$ species which is the only RO$_2$ represented in the MCM. Coloured boxes indicate species that were observed by the VOCUS PTR-MS instrument. Though nitrate carbonyl products (NC$_4$CHO) cannot be formed from this specific nitrate β-RO$_2$ from isoprene, they are formed from other nitrate radicals and thus nitrate carbonyls were also observed by the VOCUS PTR-MS instrument.

isoprene with NO$_3$ (Section 2.1). Therefore, measured RO$_2$ concentrations, which are maximum around 1×10^9 cm^{-3} (Fig. 1

265 and 2, Panel (d)), need to be regarded as lower limits.

In all experiments, significant amounts (up to 1 ppv) of methyl vinyl ketone (MVK) and methacrolein (MACR) were detected by the VOCUS PTR-MS instrument.

VOCUS PTR-MS, Br$^-$-CIMS and I$^-$-CIMS instruments also recorded ion signals from oxygenated organic compounds in the experiments that can be attributed to the sum formulas of a number of other product species including non-nitrate (HPALD:

270 C$_5$H$_8$O$_3$) and nitrate organic compounds (NISOPOOH: C$_5$H$_9$NO$_5$, NC$_4$CHO: C$_5$H$_7$NO$_4$, ISOPCNO$_3$: C$_5$H$_9$NO$_4$) and epoxide products that are expected to be formed subsequent to the ring-closure reaction of alkoxy radicals (Reaction R9, R17, C$_5$H$_8$O$_4$, C$_5$H$_8$O$_3$, C$_5$H$_9$NO$_6$, C$_5$H$_9$NO$_5$, C$_5$H$_7$NO$_5$, Fig. 6).

Ion signals shown in Fig. 4, 5, A5, A6 were the highest signals observed in the mass spectrometer instruments except for the ion signal corresponding to a C$_4$H$_7$NO$_5$ compound observed by the I$^-$- and Br$^-$-CIMS instruments. A species with this sum

formula cannot be attributed to a major product species expected from the chemical mechanism. This is discussed in detail in Tsiligiannis et al. (2022).

Signals at the mass corresponding to NISOPOOH were highest among all product signals observed by the VOCUS PTR-MS instrument. The signal can include nitrate epoxides that are produced from the ring-closure reactions of alkoxy radicals (Section 5.3) and from the reaction of NISOPOOH with OH. However, the contribution of nitrate epoxides from the ring-closure reactions to the sum of product concentrations from both reactions is expected to be low in the experiments in this work, specifically in the experiment on 09 August 2018 (Experiment #1), when HO_2 concentrations favoured $RO_2 + HO_2$ reactions and an OH scavenger was present (Fig. 4, Panel (a)). Fragmentation, though, may reduce the sensitivity of the VOCUS PTR-MS instrument for NISOPOOH at the corresponding mass as shown by Li et al. (2022) for other hydroperoxide species.

Signals from all three mass spectrometry instruments (Fig. A7, A8, A9, A10) can be compared by scaling them to best match modelled concentrations of organic products applying the FZJ-NO3 chemical mechanism.

The relative behaviour of signals is similar for all instruments with a few exceptions: (1) In the experiment on 09 August 2018 (Experiment #1), the signals of the Br^--CIMS instrument appear to be systematically lower after 10:00 UTC for unknown reasons (Fig. A7). (2) In the experiment on 13 August 2018 (Experiment #4), the loss rate of $C_5H_9NO_4$ compounds appears to be slower in the signal of the Br^--CIMS instrument than in the other mass spectrometer instruments (Fig. A10, Panel (c)) and expected from model calculations. This could be explained if other (fragments of) products were detected at that mass by the Br^--CIMS instrument, but not by the other instruments. (3) The loss rate of $C_5H_{10}O_3$ compounds observed by the I^--CIMS instrument appears to be faster than observed by the VOCUS PTR-MS instrument and expected from model calculations in the experiment on 13 August 2018 (Experiment #4) (Fig. A10, Panel (f)). The difference in the observed temporal evolution of $C_5H_{10}O_3$ compounds could be explained if the sensitivity of the instrument was lower for the hydroperoxide species than for the epoxide species, both of which are detected at the same mass (Section 5.5). Differences would become most obvious during this part of the experiment because these compounds have vastly different chemical lifetimes with respect to the reaction with OH, which was likely the dominant loss process for this part of the experiment. In some parts of the experiments, measurements by the I^--CIMS instrument exhibited an oscillating behaviour, which is most likely an instrumental artefact (for example Fig. A10, Panel (b)).

Some species produced from different loss pathways can be structurally different but have the same sum formula. These isomers cannot be distinguished by the mass spectrometers (Fig. 6): (1) Nitrate hydroperoxides (NISOPOOH) have the same mass as some nitrate epoxide species (Reaction R16). This applies for nitrate epoxides formed from the reaction of OH with NISOPOOH, which does not play a major role for conditions of the experiments, but also for specific nitrate epoxide products formed subsequently to the ring-closure reaction of nitrate alkoxy radicals predicted by the FZJ-NO3 mechanism (Vereecken et al., 2021). (2) Hydroperoxy aldehydes (HPALD) produced from unimolecular 1,6-H-shift reactions of the nitrate Z-δ-RO_2 isomers have the same mass as one epoxide product formed also from the ring-closure reaction of nitrate alkoxy radicals (sum formula $C_5H_8O_3$, Reaction R14). NO_2 is eliminated, so that these products do not contain nitrate functional groups.

The temporal behaviour of products depends on their production and destruction rates. They are formed from the same pool of nitrate RO_2 radicals from the reaction of isoprene with NO_3 which is the rate limiting step for their production. The temporal evaluation of their concentrations at later times of the experiment when isoprene had been consumed is determined by the rate of loss processes, which can be chemical loss and dilution in these experiments.

Mainly measurements by the VOCUS PTR-MS instrument are discussed in the next sections. However, the conclusions do not depend on the choice of the instrument as can be seen by the overall good agreement in time-series of ion signals at the same mass of instruments (Fig. A7, A8, A9, A10). Results are also independent on the choice of scaling measured ion mass signals of the VOCUS PTR-MS instrument to the model results of the FZJ-NO3 mechanism (A11).

5 Discussion

5.1 Chemical lifetime of nitrate RO_2 radicals

Using the RO_2 chemistry as implemented in the FZJ-NO3 mechanism and measured HO_2 concentrations results in overall loss rates of nitrate RO_2 of around 0.035, 0.005, 0.008 and $0.014\,s^{-1}$ in the experiments on 09, 10, 12, and 13 August 2018 (Experiment #1, #2, #3, #4). This implies chemical lifetimes between $30\,s$ and several minutes, which are similar to values at atmospheric night-time conditions. RO_2 loss rates are 20 to 50 % lower if the chemistry implemented in the Caltech mechanism or MCM is applied.

Overall, differences of the RO_2 loss rates derived from the three mechanisms are mainly related to differences of the distribution of nitrate RO_2 isomers, for which chemical lifetimes vary. In addition, implementation of unimolecular RO_2 reactions shorten their chemical lifetime in the FZJ-NO3 mechanism (Fig. 3, 6). Differences of RO_2 loss rates between the chemical mechanisms are lowest for the experiment on 09 August 2018 (Experiment #1), in which the RO_2 loss is dominated by the reaction with HO_2 (Fig. 7, A3). In this experiment, the overall loss rate was highest, so that unimolecular RO_2 reactions implemented in the FZJ-NO3 mechanism were less competitive.

If HO_2 concentrations are used as derived from model calculations, the total RO_2 loss rates are lower by 30 to 50 % than shown here due to the low predicted HO_2 concentrations (Vereecken et al., 2021). The contribution of the different RO_2 loss channels shifts towards higher contributions from RO_2 reactions with other RO_2 radicals and with NO_3 (Fig. A4). In addition, unimolecular reactions further gain in importance due to the longer chemical lifetime of RO_2 radicals.

5.2 Production of nitrate alkoxy radicals

Alkoxy radicals play an important role in determining the differences in the concentrations of organic products, obtained by model calculations applying the three mechanisms (Fig. 4, 5, A5, A6). These differences are not only due to differences in the fate of alkoxy radicals, but also due to differences in the formation rates of alkoxy radicals which are formed from nitrate RO_2 radicals reacting with NO_3, RO_2, and HO_2 radicals.
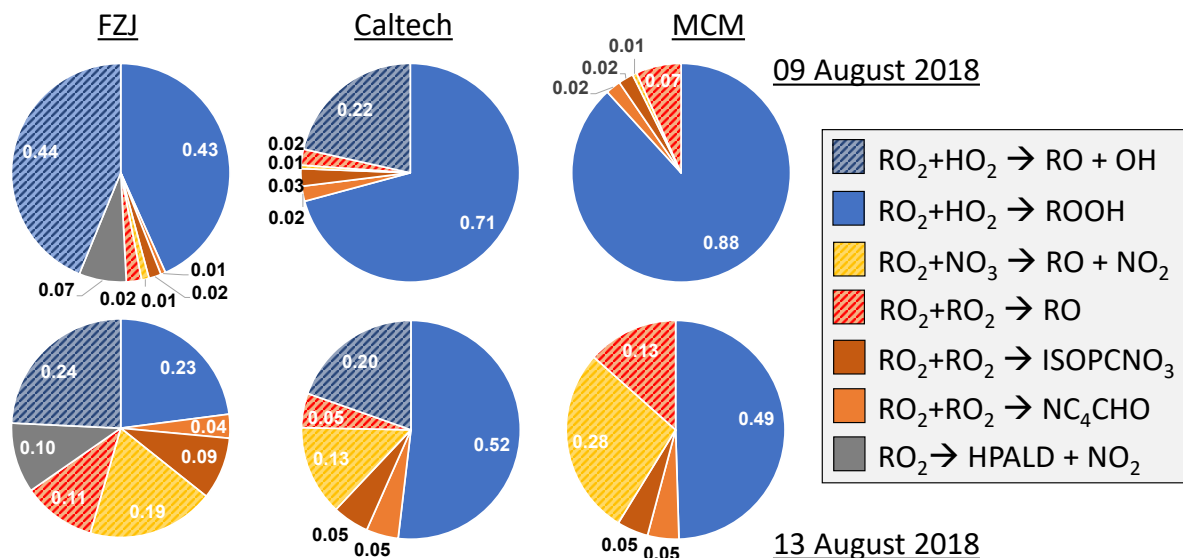
Figure 7. Relative distribution of loss rates of nitrate RO_2 for the experiment on 09 August 2018 (Experiment #1), when HO_2 concentrations were enhanced, and for the experiment on 13 August 2018 (Experiment #4), when the amount of oxidized isoprene was highest. The total RO_2 loss rate was 0.035 and 0.014 s^{-1} in the experiment on 09 August 2018 (Experiment #1) and 13 August 2018 (Experiment #4), respectively. Calculations of the loss rates of RO_2 radicals in bimolecular reactions make use of measured HO_2 and NO_3 concentrations. Total RO_2 concentrations and concentrations of speciated nitrate RO_2 were derived from model calculations applying either the FZJ-NO3, Caltech or MCM mechanism. The chemical mechanisms differ with respect to the number of nitrate RO_2 isomers that are considered, the type of RO_2 loss reactions and products of loss reactions (Fig. 3 and 6). Reactions leading to nitrate alkoxy radicals are indicated by a dotted pattern.

In all three mechanisms, the initial product from the reaction between nitrate RO_2 and NO_3 is a nitrate alkoxy radical and
340   NO_2 (Fig. 6, Reaction R3). Dewald et al. (2020) analysed NO_3 reactivity measurements performed in the same experiments and concluded that the reaction rate constant of the reaction of nitrate RO_2 with NO_3 would need to be around $5 \times 10^{-12} \, cm^3 s^{-1}$, which is nearly a factor of 2 higher than the generic reaction $RO_2 + NO_3$ rate constant based on the measured rate constant for $CH_3O_2 + NO_3$ used in the MCM and the Caltech mechanisms. With this rate constant, the loss rate of nitrate RO_2 in the reaction with NO_3 is between 0.001 and 0.003 s^{-1} in the experiments on 10, 12 and 13 August 2018 ((Experiment #2, #3, #4),
345   contributing between 5 and 20 % of the total nitrate RO_2 loss rate if the FZJ-NO3 mechanism is applied (Fig. 7, A3).

Rate constants of $RO_2 + RO_2$ reactions for nitrate RO_2 in the Caltech mechanism were derived from the measurement of isomer specific product distributions in the experiments of Schwantes et al. (2015). From their findings, a reaction rate constant of $7 \times 10^{-14} \, cm^3 s^{-1}$ for the self- and cross-reaction of the most abundant nitrate β-1,2-RO_2 radical was found. As this rate refers to a tertiary radical instead of a primary, it is significantly slower than the rate constant used in the MCM of
350     $1.3 \times 10^{-12} \, cm^3 s^{-1}$. Rate constants for other nitrate RO_2 were estimated in the Caltech mechanism to be in the range of 10^{-12} and $10^{-13} \, cm^3 s^{-1}$. In the FZJ-NO3 mechanism, all the rates for the nitrate RO_2 self- and cross-reactions were calculated from

structure activity relationship (Jenkin et al., 2019) resulting in an even lower rate constant for the self- and cross-reaction of the tertiary β-1,2-RO_2 of only 3×10^{-16} cm^{3}s^{-1} and for the cross-reactions of this radical with other primary nitrate RO_2 of 2 to 10×10^{-14} cm^{3}s^{-1}. The rates of the reactions within the pool of the other nitrate RO_2 are on the same order of magnitude as the values in the Caltech mechanism.

355

Only RO_2 concentrations derived from model calculations can be used to estimate the loss rate of nitrate RO_2 in $RO_2 + RO_2$ reactions (=alkoxy radical production rate) because the instrument detecting RO_2 could only measure low limit concentrations (Vereecken et al., 2021). This gives average RO_2 loss rates between 0.0005 s^{-1} and 0.002 s^{-1}. The contribution to the total loss rate is less than 10 % in the experiments on 09, 10, 12 August 2018 (Experiment #1, #2, #3, #4) but increased to up to

360   20 % in the experiment on 13 August 2018 (Experiment #4), when also the production rate of nitrate RO_2 was highest (Fig. 7).

A yield of 60 % for the formation of alkoxy radicals (Fig. 6, Reaction R4) is generally applied for RO_2+RO_2 radical reactions for primary and secondary RO_2 (Jenkin et al., 2019). In the case of the most abundant nitrato-organic peroxy radical (tertiary β-1,2-RO_2) from the reaction of isoprene with NO_3, however, the yield is nearly 100 % for its self-reaction and 80 % if this nitrate RO_2 reacts with other RO_2 because the formation of a nitrate carbonyl product (NC_4CHO) is not possible (Fig. 6,

365   Reaction R5). Formation of peroxides ($ROOR$) is considered in the Caltech and FZJ-NO3 mechanisms with a small yield of 3.5 %. The MCM does not distinguish between nitrate RO_2 isomers. Therefore, this increase in the yield of alkoxy radicals is only implemented in the Caltech and FZJ-NO3 mechanisms. With respect to the total yield of alkoxy radicals, the high yield for the β-RO_2 is partly compensated by the lower rate constants of RO_2+RO_2 radical reactions in the FZJ-NO3 and Caltech mechanisms than applied in the MCM.

370   As discussed in Schwantes et al. (2015), reactions of nitrate β-RO_2 and HO_2 can also result in the formation of nitrate alkoxy radicals together with an OH radical (Fig. 6, Reaction R2). A yield of 50 % is assumed in the Caltech and FZJ-NO3 mechanisms (Section 5.3).

Overall, the total yield of alkoxy radicals produced in the reactions of nitrate RO_2 differ significantly between the 3 mechanisms. In the FZJ-NO3 mechanism, the total yield is around 50 %. The value is similar in all experiments analysed in this

375   work, but the type of reactions producing the alkoxy radicals shifts depending on the availability of reaction partners (Fig. 7). Alkoxy radicals yields are 25 and 40 % lower in the Caltech mechanism than in the FZJ-NO3 mechanism. The value is mainly due to the shift in the RO_2 isomer distribution towards δ-RO_2 isomers. Lowest total yields of alkoxy radicals between 7 and 40 % are obtained if the MCM is applied because the MCM does not include alkoxy radical production from the reaction of nitrate RO_2 with HO_2.

380   ## 5.3 Fate of nitrate alkoxy radicals

The fate of the alkoxy radicals is very different between the three mechanisms which impacts the distribution of organic products. In the MCM, the only pathway for nitrate alkoxy radicals produced from isoprene is their decomposition forming a nitrate carbonyl (NC_4CHO) together with an HO_2 radical (Fig. 6, Reaction R7). This pathway is not possible for the alkoxy radical from the β-RO_2 radicals, which are absent in the MCM mechanism but included in the FZJ-NO3 and Caltech

mechanisms. Therefore, the overall yield of nitrate carbonyls (NC_4CHO) from the subsequent chemistry of nitrate alkoxy radicals is highest if the MCM mechanism is applied in comparison to the results from the other 2 mechanisms.

In the Caltech mechanism, alkoxy radicals from β-RO_2 radicals decompose exclusively to MVK or MACR together with a formaldehyde and an NO_2 molecule (Fig. 6, Reaction R8 Wennberg et al. (2018)). Therefore, nitrate carbonyl concentrations predicted by the Caltech model are at least a factor of 4 lower than calculated when applying the MCM. Small concentrations of nitrate carbonyls are also produced from reactions of nitrate δ-RO_2 radicals.

Vereecken et al. (2021) calculated that ring-closure reactions leading to the formation of nitrate epoxy alkyl radicals are much faster than the decomposition reaction for the nitrate β-RO alkoxy isomer Fig. 6, Reaction R9, R17), so that MVK and MACR production from this reaction is suppressed. Products from the epoxide pathway are discussed in Section 5.4. Differences between NC_4CHO concentrations predicted by the FZJ-NO3 and Caltech mechanism are due to differences in the initial distribution of nitrate RO_2 isomers. The FZJ-NO3 mechanism favours the β-1,2-RO_2 radicals (Section 3) that do not produce NC_4CHO and overall react slower with other RO_2 than with the other nitrate RO_2 radicals.

The VOCUS PTR-MS instrument detected ion signals at the expected mass of NC_4CHO with the sum formula $C_5H_7NO_4$ in all experiments. Due to the lack of calibration, this measurement cannot be used to test the validity of any of the three chemical mechanisms. However, NC_4CHO concentrations would be roughly consistent with predictions by the Caltech and FZJ-NO3 mechanisms if a sensitivity similar to that for ketones without nitrate functional groups (acetone, MVK, pentanone, nopinone) is assumed.

MVK and MACR are formed in all three mechanisms from the oxidation of isoprene by OH and ozone. Yields from the ozonolysis of isoprene are 0.17 and 0.41 for MVK and MACR, respectively (Nguyen et al., 2016). In the absence of NO as for typical night-time conditions, MVK and MACR are produced from the reaction of OH derived RO_2 radicals with other RO_2 or HO_2 radicals. The overall yield of MVK from the OH oxidation of isoprene in experiments in this work depends on the fate of RO_2 radicals, but is expected to be small due to the slow $RO_2 + RO_2$ reaction rate and small yields in the range of a few percent from the $RO_2 + HO_2$ reaction (Wennberg et al., 2018). In addition to the production from OH and O_3 reactions, the Caltech mechanism includes a strong source for MVK through the decomposition of nitrate β-1,2-RO_2 radicals produced from the NO_3 oxidation.

In all experiments, analysed in this work, measured MVK and MACR concentrations are consistent with predictions by the MCM and FZJ-NO3 mechanisms (Fig. 4, 5). In contrast, predictions by the Caltech mechanism are up to a factor of 2 to 4 higher than measured values. Discrepancies are highest in experiments in which a high fraction of the nitrate alkoxy radicals are formed from the reaction of nitrate RO_2 with NO_3 with an alkoxy radical yield of 1 (13 August 2018, Fig. 5) and are lowest in the experiment in which nitrate RO_2 mainly reacted with HO_2 (09 August 2018, Fig. 4). The good model-measurement agreement for MVK+MACR concentrations obtained using the FZJ-NO3 and MCM mechanisms confirms that the decomposition of the nitrate alkoxy radicals is negligible as predicted by Vereecken et al. (2021) and unlike predicted by the Caltech mechanism.

5.4 Epoxide products from ring-closure reactions of nitrate alkoxy radicals

Epoxide formation from ring-closure reactions of nitrate alkoxy radicals leading to epoxy-RO_2 radicals is implemented only in the FZJ-NO3 mechanism (Fig. 6, Reaction R9, R17, Vereecken et al. (2021)).

Nitrate epoxides can be formed from bimolecular reactions of epoxy-RO_2 radicals with RO_2 and HO_2 (Fig. 6, Reaction R12, R16, R19, R26) and from nitrate epoxy alkoxy radicals produced by the reaction of epoxy-RO_2 radicals with NO_3 (Fig. 6, Reaction R13, R21). One of the epoxy-RO radicals exclusively undergoes a 1,5-H-shift reaction for conditions of the experiments and decomposes to an epoxide and NO_2 (Fig. 6, Reaction R14). Another epoxy-RO radical can decompose into a C_5 nitrate epoxide releasing HO_2 (Fig. 6, Reaction R22). This reaction competes with a 1,5-H-shift reaction, in which a C_4 nitrate together with an HO_2 radical and formaldehyde (HCHO) are formed (Fig. 6, Reaction R23).

Epoxy-RO_2 can also undergo unimolecular reactions (Vereecken et al., 2021) that compete with bimolecular reactions. The fastest unimolecular reaction is a 1,6-H-shift reaction with a rate constant of $3.7 \times 10^{-3}\,\mathrm{s}^{-1}$ at room temperature leading to a C_5 epoxy product ($C_5H_8O_4$) together with NO_2 (Fig. 6, Reaction R11). This loss rate is lower than the loss rate due to bimolecular reactions, which are on the order of $10^{-2}\,\mathrm{s}^{-1}$ for conditions of the experiments in this work but high enough that low concentrations of this epoxide product may be formed (Fig. 5, Panel (f)).

The mass spectrometer instruments cannot distinguish between hydroxy nitrate epoxides formed from the reaction of epoxy-RO_2 radicals with other RO_2 radicals and nitrate hydroperoxides (NISOPOOH) because they have the same sum formula, $C_5H_9NO_5$. The concentration of epoxide $C_5H_9NO_5$ species is expected to be at most 30 to 40 % of the concentration of NISOPOOH in the experiment on 13 August 2018 (Fig. 5), when RO_2 concentrations were highest. Their concentration is expected to be less than 10 % of NISOPOOH in the experiment on 09 August 2018 (Fig. 4, Panel (a)), when RO_2 reactions with HO_2 dominated the overall RO_2 loss. Therefore, ion mass signals corresponding to $C_5H_9NO_5$ species cannot be used to estimate the importance of the epoxidation reaction pathways.

Bimolecular reactions of epoxy-RO_2 can also lead to the formation of products with sum formulas that are specific for the epoxidation chemistry. Different isomers of nitrate carbonyls with the sum formula $C_5H_7NO_5$ are produced from reactions of epoxy-RO_2 with other RO_2 radicals or with NO_3 (Fig. 6, Reaction R19, R22). In addition, $C_5H_9NO_6$ compounds are formed from reactions of nitrate epoxy-RO_2 with HO_2 (Fig. 6, Reaction R12, R26). Mixing ratios of these epoxides are predicted to be highest with mixing ratios of $1\,\mathrm{ppbv}$ in the experiment on 13 August 2018 (Experiment #4), when the total isoprene consumption by NO_3 reactions was highest. Values are similar to mixing ratios of other products obtained in this experiment (Fig. 5, Panel (g)).

The mass spectrum measured by the VOCUS PTR-MS instrument shows clear signals at the masses of epoxy nitrate compounds. The count rates are much lower than signals of other products, although expected concentrations are in the same range. This could be due to a lower sensitivity of the instrument for nitrate epoxides than for other organic nitrates. However, this could also indicate a lower than assumed production rate of alkoxy radicals for example from the reaction of nitrate RO_2 with HO_2 (Section 5.5).

A C_4-nitrate with the sum formula $C_4H_5NO_4$ produced subsequent to the 1,5-H reaction of the nitrate alkoxy radical (Fig. 6, Reaction R23–R25) was not detected by the VOCUS PTR-MS instrument in the experiments in this work, though significant mixing ratios of up to 0.6 ppbv are calculated by the FZJ-NO3 mechanism in the experiment on 13 August 2018 (Experiment #4), when the amount of oxidized isoprene was highest (Fig. 5, Panel (i)). There is no obvious reason why the sensitivity of the instrument for this compound would be lower than for other compounds. Only the I^- CIMS instrument detected a very small signal (less than 30 cnts) at the corresponding mass , which is at least a factor of 100 smaller than ion signals of masses at other products shown in Fig. A10).

The formation of this compound competes with the decomposition of the epoxy alkoxy radical leading to an epoxy-C_5 compound with the sum formula $C_5H_7NO_5$ that is observed in the mass spectrum of the VOCUS PTR-MS instrument (Fig. 6, Reaction R22). The fact that the C_4 nitrate is not observed in the mass spectrum could indicate that the 1,5-H reaction is not competitive or that the branching ratio of 2 epoxy-alkyl radicals from the nitrate alkoxy radical disfavours the epoxy-alkyl radical that eventually leads to the formation of the C_4 nitrate (Fig. 6, Reaction R17). Rate constants of the epoxidation chemistry calculated in Vereecken et al. (2021) have an uncertainty of a factor of 2 to 4. Therefore, low rate constants that weaken the formation of the C_4 nitrate are within in the uncertainty of calculations.

The other epoxy compound without a nitrate functional group is produced from a 1,6-H-shift reaction of one of the nitrate epoxy-RO_2 (Fig. 6, Reaction R11). Due to the relatively low reaction rate constant, only small mixing ratios of maximum 0.15 ppbv of this compound with the sum formula $C_5H_8O_4$ are modelled for the experiment on 13 August 2018 (Experiment #4) (Fig. 5, Panel (f)). Nevertheless, a corresponding signal is observed in the mass spectrum of the VOCUS PTR-MS instrument.

5.5 Reaction of nitrate RO_2 with HO_2

The chemical loss rates of nitrate RO_2 towards reaction with HO_2 was $0.032\,s^{-1}$ (90 % of the total loss rate) in the experiment with high HO_2 concentrations (09 August 2018, Experiment #1). The contribution to the total loss rate was 40 to 50 % with loss rates between 0.002 and $0.007\,s^{-1}$ in the other experiments (Fig. 6). In general, this reaction can proceed via several reaction pathways (Rollins et al., 2009; Kwan et al., 2012; Schwantes et al., 2015):

$$nitrate - RO_2 + HO_2 \quad \rightarrow \quad ROOH + O_2 \qquad (R1)$$

$$nitrate - RO_2 + HO_2 \quad \rightarrow \quad RO + OH + O_2 \qquad (R2)$$
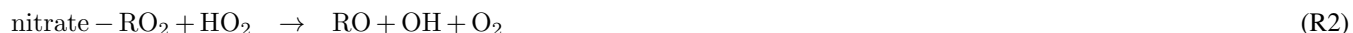
Nitrate hydroperoxide (NISOPOOH) is the only product in the MCM (Reaction R1) and a major product in the Caltech and FZJ-NO3 chemical mechanisms (Fig. 6, Reaction R1). The Caltech and FZJ-NO3 mechanisms assume that the yield of nitrate alkoxy radicals is approximately 0.5 if nitrate β-RO_2 radicals react with HO_2 (Reaction R2). The fate of nitrate alkoxy radicals is discussed above (Section 5.3). Predictions of NISOPOOH concentrations by the three mechanisms differ significantly. NISOPOOH concentrations predicted by the FZJ-NO3 mechanism are approximately half of the concentration calculated by the MCM and concentrations predicted by the Caltech mechanism are between both values. This is mainly due to the different distribution of nitrate β- and δ-RO_2 radicals in the FZJ-NO3 and Caltech mechanisms.
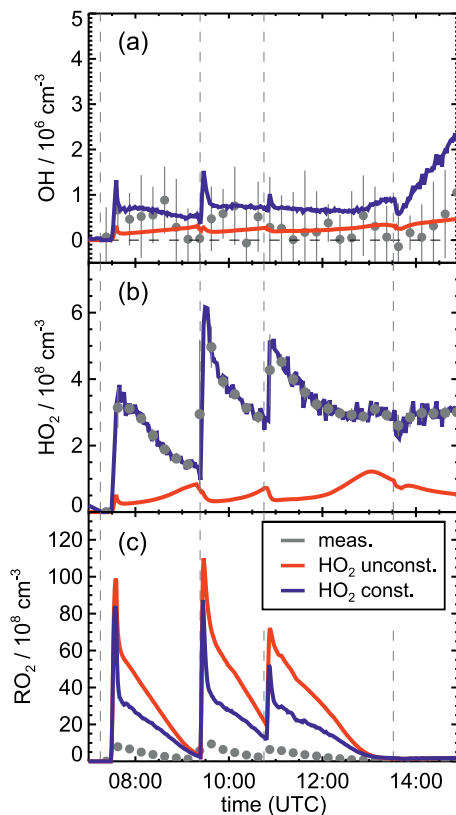
Figure 8. Comparison of results from model calculations applying the FZJ-NO3 mechanism for the experiment on 13 August 2018 (Experiment #4) with HO_2 concentrations being either constrained or unconstrained to measurements. A large fraction of OH is produced from the reaction of HO_2 with NO_3, so that lower than measured HO_2 concentrations in the unconstrained model run lead to low OH concentrations. Because HO_2 + RO_2 reactions contribute significantly to the total loss of RO_2, modelled RO_2 concentrations are higher in the unconstrained model run. RO_2 measurements by the LIF instrument does not include all RO_2 radicals (Vereecken et al., 2021), so that measured concentrations are lower than modelled values.

The VOCUS PTR-MS instrument was not calibrated for NISOPOOH, so that its concentrations could not be determined.
485 The high count rate observed by this instrument and the 2 other CIMS instruments and the uncertainty in the branching ratio of Reactions R1 and R2 appear to support a high yield of NISOPOOH from the reaction of HO_2 with nitrate RO_2.

Alkoxy radical formation from the reaction of nitrate RO_2 with HO_2 is accompanied by the formation of OH (Fig. 6, Reaction R2), which can be responsible for the formation of products that are specific for the OH oxidation of isoprene as observed in experiments designed to investigate the NO_3 oxidation mechanism of isoprene.
490 OH concentrations were measured in the experiments in this work, but concentrations were around the limit of detection of the instrument (a few $10^5 \, cm^{-3}$) in most experiments. Model calculations for the experiment on 13 August 2018 (Experiment #4), when reactant concentrations were highest, result in significant OH concentrations between 5 and $8 \times 10^5 \, cm^{-3}$ and also

model results indicate that OH concentrations could have been in the range of a few $10^5\,\mathrm{cm}^{-3}$ (Fig. 5, Panel (j)). A large fraction of OH, however, is produced by the reaction of HO_2 with NO_3, both of which are constrained to measured values in the model calculations. As discussed in Vereecken et al. (2021), model calculations without constraining HO_2 to measured values cannot reproduce measured HO_2 concentration suggesting shortcomings of the model to describe HO_2 source and/or sink reactions.

This is further analysed by comparing results of model runs, in which either HO_2 concentrations are constrained to measurements or HO_2 is calculated by the model (Fig. 8). In the unconstrained case, modelled HO_2 concentrations are much lower than measurements. This reduces the OH concentration by a factor of 3 due to the lower production of OH from the reaction of HO_2 with NO_3. During the part of the experiment, when isoprene is oxidized by NO_3, differences between measured and modelled OH concentrations tend to be smaller if HO_2 is not constrained to measured values. At later times of the experiment after 13:30 UTC, when isoprene had been consumed and NO_3 concentrations were enhanced by additional injections of NO_2 and O_3 (Fig. 2, Panel (b)), measurements show a steeper increase of OH concentrations than model calculations with unconstrained HO_2. This further indicates that modelled HO_2 concentrations might be too low.

If the yield of alkoxy radicals and therefore also of OH from the reaction of nitrate RO_2 with HO_2 was lower than $50\,\%$ as assumed in the Caltech and FZJ-NO3 mechanisms, modelled OH concentrations would be even lower. Sensitivity model runs show that modelled OH concentrations would only decrease by 1 to $3 \times 10^5\,\mathrm{cm}^{-3}$ directly after the isoprene injections, when nitrate RO_2 concentrations are also highest. However, such differences are in the range of the accuracy of measurements, which was a few $10^5\,\mathrm{cm}^{-3}$ due to the subtraction of an OH background signal that was determined by using a chemical modulation system (Cho et al., 2021).

Overall, considering the uncertainties in the measured OH concentrations and in the modelled OH due to the uncertainty in the OH production from the $HO_2 + NO_3$ reaction, differences between model results and measured values are too small to draw conclusions about the yield of alkoxy radicals from model-measurement comparison of OH concentrations.

5.6 Production of hydroperoxy aldehydes (HPALD) from nitrate RO_2 isomerization reactions

Only the FZJ-NO3 mechanism includes unimolecular loss reactions of nitrate RO_2 (Fig. 3). The reaction rate constants of the 1,6-H shift reactions of the Z-δ-RO_2 isomers have a strong temperature dependence (Vereecken et al., 2021). Values range between 0.016 to $0.023\,\mathrm{s}^{-1}$ for the Z-δ-1,4-RO_2 isomer and 0.045 and $0.06\,\mathrm{s}^{-1}$ for the Z-δ-4,1-RO_2 isomer for temperatures experienced in the experiments in this work.

The fraction of Z-δ-RO_2 isomer to the total RO_2 concentration is only between 5 and $6\,\%$ and between 1 and $2\,\%$ for the Z-δ-4,1-RO_2 isomer. The overall bulk RO_2 isomerization rate is around $0.002\,\mathrm{s}^{-1}$ making the 1,6-H-shift reaction competitive with bimolecular reactions in all experiments except for the one with high HO_2 concentrations (09 August 2018, Experiment #1). The contribution of unimolecular reactions to the overall loss rate is expected to be between 10 and $30\,\%$ depending on the total RO_2 loss rate (Fig. 7). This is similar or even higher than for analogous, much faster 1,6-H-shift reactions in the OH-initiated isoprene oxidation ($k(298\,\mathrm{K}) \approx 0.5\,\mathrm{s}^{-1}$, Peeters et al. (2014)) due to significantly longer RO_2 lifetimes during the night than during the day.

HPALD concentrations predicted by the model applying the FZJ-NO3 mechanism are between 0.1 and 1.2 ppbv depending on the chemical conditions with different availability of reaction partners for competing bimolecular reactions. HPALD mixing ratios are calculated to be highest in the experiment on 13 August 2018 (Experiment #4), when the total concentration of oxidized isoprene was high. Approximately 10 to 15 % of the HPALD that is predicted by the FZJ-NO3 mechanism is due to OH oxidation of isoprene also producing HPALD from 1,6-H-shift reactions. The modelled HPALD concentration from the OH reactionmight be less, however, due to the uncertainty of the modelled OH concentration (Section 5.5). It is worth noting that the fast 1,6-H-shift reactions rate of Z-δ-RO_2 isomers from the OH oxidation of isoprene (bulk loss rate $\approx 0.006\,s^{-1}$) makes these reactions very competitive with bimolecular reactions for night-time conditions (loss rate in the experiments in this work: 0.005 to $0.014\,s^{-1}$, Section 5.1).

Although the absolute importance of HPALD formation from H-shift reactions of nitrate RO_2 radicals is uncertain, HPALD is clearly formed from the oxidation of isoprene by NO_3. This is demonstrated by the observation of a signal at the mass of HPALD in the experiment on 09 August 2018 (Experiment #1), when an OH scavenger was present, so that HPALD could not be produced by OH reactions. In this experiment, $HO_2 + RO_2$ reactions were favoured, so that also formation of the epoxides with the same mass is expected to be small (Fig. 4, Panel (c)). Therefore, the signal on the mass of HPALD can be attributed to HPALD formation from the oxidation of isoprene by NO_3 in this experiment.

The relative importance of HPALD formation is expected to be highest for conditions of the experiment on 10 August 2018 (Experiment #2), when the total loss rate of RO_2 due to bimolecular reaction is between 0.005 and $0.006\,s^{-1}$. In this case, approximately 25 to 30 % of the isoprene consumed by NO_3 would form HPALD. Brownwood et al. (2021) calculated the yield of total organic nitrates from measurements for the same experiments analysed in this work and found a yield of (94 ± 20) % for this experiment. Values ranged between (112 ± 13) % and (140 ± 24) % in the other experiments. The lowest yield of organic nitrates is obtained in the experiment with the longest RO_2 lifetime (10 August 2018, Experiment #2) supporting that more non-nitrate organic products such as HPALD are formed in this experiment than in the other experiments. The signal of the VOCUS PTR-MS instrument, however, does not clearly scale with the expected differences in the HPALD concentrations predicted for the experiments in this work. This and the overall high yields of organic nitrates indicate that the impact of unimolecular reactions producing HPALD might be overestimated in the FZJ-NO3 mechanism. Uncertainties in the quantum-chemical calculations, from which reaction rates are taken, are a factor of 2 to 3.

Overall, experiments in this work and previous chamber experiments demonstrate that HPALD formation from 1,6-H shift reactions of Z-δ RO_2 isomers play a role for atmospheric night-time conditions.

5.7 Night-time loss rate of organic nitrate products and hydroperoxy aldehydes (HPALD)

Chamber experiments in this work were designed to also investigate further oxidation of the organic products. This was achieved by re-injecting O_3 and NO_2 to enhance NO_3 production after most of the isoprene had reacted away (Fig. 2, 1, Panel (a)). Highest product concentrations were achieved in the experiment on 13 August 2018 (Experiment #4), when the amount of isoprene that was oxidized was highest. Therefore, the further discussion concentrates on this experiment (Fig. 5).

Reaction rate constants of nitrate products from the oxidation of isoprene with OH and O_3 implemented in the Caltech mechanism are based on laboratory experiments with synthetic standards of isoprene hydroxy nitrate isomers (Wennberg et al., 2018; Lee et al., 2014b). Values are assumed to be applicable for other organic nitrates such as nitrate carbonyls and nitrate hydroperoxides. Only part of the loss reactions listed in Wennberg et al. (2018) are implemented in the code of the Caltech mechanism (Bates and Wennberg, 2017) that is applied in model calculations in this work.

Rate constants for the reaction of the first generation organic nitrates with ozone (Reaction R28, R31, R34, R37) are in the range of 10^{-17} to $10^{-19}\,\mathrm{cm^3\,s^{-1}}$ in Lee et al. (2014b) with rates being relevant for only δ-nitrate alcohols and -hydroperoxides for typical oxidant concentrations during the night but too slow for β-species. As only δ-species are implemented in the MCM, the overall relevance of ozonolysis loss reactions are overestimated under atmospheric conditions in the MCM (Table 2).

In the FZJ-NO3 mechanism, reaction rate constants of organic nitrates with OH radicals (Reaction R27, R30, R33, R36) are taken from the Caltech mechanism, but rate constants with ozone and NO_3 are optimized to best describe the temporal behaviour of the signals observed by the VOCUS PTR-MS instrument at the respective mass (Table 2). Reaction rate constants of loss reactions that lead to loss rates much lower than the dilution rate of the chamber, are set to upper limit values that equal the loss rate due to dilution ($k_{dil} = 1.5 \times 10^{-5}\,\mathrm{s^{-1}}$). Reaction rate constants are likely even lower because doubling the loss rate from dilution would already worsen the model-measurement agreement of the temporal behaviour of products.

Chemical loss of NISOPOOH by reactions with NO_3 (Reaction R29) and O_3 (Reaction R28) are expected not to be relevant for atmospheric conditions in all mechanisms. This is consistent with the slow decay of the total signal for $C_5H_9NO_5$ observed by the VOCUS PTR-MS instrument in the experiment on 09 August 2018 (Experiment #1), when OH oxidation was suppressed by the presence of an OH scavenger (Fig. 4, Panel (a)). In this case, the loss rate is consistent with the dilution rate in the experiment.

In the MCM, the rate of the reaction of OH with hydroperoxides, NISOPOOH, is assumed to be fast with a rate coefficient of $10^{-10}\,\mathrm{s^{-1}\,cm^3}$. In contrast, the Caltech and FZJ-NO3 mechanisms assume a smaller rate coefficient for this reaction, by a factor o 3, which can account for the faster decay of NISOPOOH in the MCM mechanism than in the Caltech and FZJ-NO3 mechanisms.

In the MCM, products of the NISOPOOH + OH reaction (Reaction R27) are a nitrate alkoxy radical together with an OH radical leading to a zero net loss of OH. In addition, the alkoxy radical produces a nitrate carbonyl (NC_4CHO) together with an HO_2 (Section 5.3). In contrast, in the Caltech and FZJ-NO3 mechanisms, a large fraction of the predicted products are epoxide products (yield: 0.37 to 1.0 depending on the precursor RO_2 isomer, Schwantes et al. (2015)) together with OH analogous to the formation of epoxides in the OH oxidation of isoprene (Paulot et al., 2009).

Nitrate epoxides have the same sum formula as NISOPOOH ($C_5H_9NO_5$), so that the VOCUS PTR-MS instrument cannot distinguish between both compounds. The reaction of OH radicals with nitrate epoxides is expected to be much slower than their reaction with NISOPOOH due to the lack of C=C double bonds. Therefore, the time series of the sum of both compounds is affected by their different temporal behaviour in the Caltech and FZJ-NO3 mechanisms. The loss rate of $C_5H_9NO_5$ compounds in the MCM is only determined by the fast loss of NISOPOOH because no epoxides are formed.

Table 2. Reaction rate constants for the reaction of first generation major organic products from the reaction of isoprene with NO_3 with OH, O_3 and NO_3 implemented in the MCM, Caltech and FZJ-NO3 mechanisms. For simplicity rate constants are given for a temperature of $T = 298\,K$ and only for the organic nitrate that is produced from the most abundant β-1,2-RO_2 radical, except for the MCM, where the δ-1,4-RO_2 is solely present. For the nitrate carbonyl (NC_4CHO). For the nitrate carbonyl (NC_4CHO), which cannot be produced from this RO_2 isomer, the value for the E-δ-1,4-RO_2 isomer is given instead. In the FZJ-NO3 mechanism, loss rates due to reactions that lead to loss rates much lower than the dilution rate of the chamber, were set to upper limit values that equal the loss rate due to dilution. Chemical lifetimes (τ) are calculated for the presence of $1 \times 10^6\,cm^{-3}$ OH, $100\,ppbv\,O_3$ and $50\,pptv\,NO_3$, which can be regarded as upper limit concentrations for typical night-time conditions. The code of the Caltech mechanism (Bates and Wennberg, 2017) includes less loss reactions implemented as described in (Wennberg et al., 2018). Chemical loss of nitrate epoxides are not implemented in the chemical mechanisms.

		MCM		Caltech		FZJ	
		$k\,/\,s^{-1}cm^3$	$\tau\,/\,h$	$k\,/\,s^{-1}cm^3$	$\tau\,/\,h$	$k\,/\,s^{-1}cm^3$	$\tau\,/\,h$
R27	$NISOPOOH + OH$	1.0×10^{-10}	2.8	3.8×10^{-11}	7.3	3.8×10^{-11}	7.3
R28	$NISOPOOH + O_3$	$-^a$		$-^{a,b}$		$< 6 \times 10^{-18}$	> 19
R29	$NISOPOOH + NO_3$	$-^a$		$-^{a,c}$		$< 3 \times 10^{-15}$	> 19
R30	$NC_4CHO + OH$	4.2×10^{-11}	6.6	4.1×10^{-11}	6.8	4.1×10^{-11}	6.8
R31	$NC_4CHO + O_3$	2.4×10^{-17}	4.6	$-^{a,d}$		$< 6 \times 10^{-18}$	> 19
R32	$NC_4CHO + NO_3$	1.2×10^{-14}	19	$-^{a,e}$		$< 3 \times 10^{-15}$	> 19
R33	$ISOPCNO_3 + OH$	1.1×10^{-10}	2.5	3.1×10^{-11}	9.0	3.1×10^{-11}	9.0
R34	$ISOPCNO_3 + O_3$	4.1×10^{-17}	2.7	$-^{a,f}$		$< 6 \times 10^{-18}$	> 19
R35	$ISOPCNO_3 + NO_3$	$-^a$		$-^{a,g}$		$< 3 \times 10^{-15}$	> 19
R36	$HPALD + OH$	5.1×10^{-11}	5.4	5.1×10^{-11}	5.4	5.1×10^{-11}	5.4
R37	$HPALD + O_3$	2.4×10^{-17}	4.6	$-^a$		$< 6 \times 10^{-18}$	> 19
R38	$HPALD + NO_3$	1.2×10^{-14}	19	$-^a$		$< 3 \times 10^{-15}$	> 19

[a] not implemented; [b] $2.8 \times 10^{-19}\,s^{-1}cm^3$, Wennberg et al. (2018); [c] $3.0 \times 10^{-14}\,s^{-1}cm^3$, Wennberg et al. (2018); [d] $4.4 \times 10^{-18}\,s^{-1}cm^3$, Wennberg et al. (2018); [e] $1.1 \times 10^{-13}\,s^{-1}cm^3$, Wennberg et al. (2018); [f] $2.8 \times 10^{-19}\,s^{-1}cm^3$, Wennberg et al. (2018); [g] $3 \times 10^{-14}\,s^{-1}cm^3$, Wennberg et al. (2018)

For the experiment on 13 August 2018 (Experiment #4) (Fig. 5, Panel (a)), the temporal behaviour of the total ion signal corresponding to $C_5H_9NO_5$ species observed by the VOCUS PTR-MS instrument fits best the modelled trace of the FZJ-NO3 mechanism with the low OH reaction rate of NISOPOOH. In addition, the low chemical loss rate of epoxides contributes to the slow decay of the ion signal at that mass improving the model-measurement agreement. This demonstrates that OH reaction rate constants measured in Lee et al. (2014b) for nitrate alcohols can be applied to NISOPOOH as implemented in the Caltech and FZJ-NO3 mechanisms. In contrast, the fast OH reaction rate constant for NISOPOOH implemented in the MCM cannot describe the observations.

If the MCM mechanism is used, a significant fraction of nitrate carbonyls, NC_4CHO, that are produced from nitrate RO_2 + RO_2 reactions and from the decomposition of specific nitrate alkoxy radicals is expected to be consumed on the time scale of the experiment for the experiment on 13 August 2018 (Experiment #4) (Fig. 5, Panel (d)). For conditions of this experiment, reactions of NC_4CHO with OH (Reaction R30) but also with NO_3 (Reaction R32) for high NO_3 concentrations can be relevant if reaction rate constants of the MCM are applied (Table 2). The loss of NC_4CHO calculated using the MCM is faster than calculated using the Caltech and FZJ-NO3 mechanisms because of the fast chemOH reaction rate constants. In addition, the MCM overestimates the loss of NC_4CHO by the reaction with ozone as discussed above.

The temporal behaviour of the modelled NC_4CHO concentrations are in good agreement with the corresponding signal observed by the VOCUS PTR-MS instrument for the Caltech and FZJ-NO3 mechanisms. This confirms that only a small fraction of NC_4CHO is expected to be chemically lost for typical night-time conditions.

In addition, a fast loss rate due to the reaction with NO_3 (Reaction R32) as suggested in Wennberg et al. (2018) would lead to a chemical lifetime of NC_4CHO of less than 30 min in the last phase of the experiment on 13 August 2018 (Experiment #4), when NO_3 mixing ratios increased to several 100 pptv (Fig. 2, Panel (b)), but this is not observed (Fig. 5, Panel (d)). Though not fully applicable, structure activity relationship in Kerdouci et al. (2014) gives reaction rate constants lower than $10^{-16}\,s^{-1}cm^3$ supporting the low loss rate due the addition of NO_3. Overall, further oxidation of nitrate carbonyls from isoprene is of minor importance for typical night-time conditions as experienced in these experiments.

Similar differences between model predictions like for NC_4CHO are seen for nitrate alcohols ($ISOPCNO_3$, Reaction R33, 34, 35): The MCM predicts a significant faster chemical loss than the Caltech and FZJ-NO3 mechanisms. A large part of the discrepancy is explained by the fast loss due to the reaction with ozone implemented in the MCM that is not applicable as discussed above. In addition, the reaction rate constant of the reaction of $ISOPCNO_3$ with OH (Reaction R33) is up to 3 times faster in the MCM than in the Caltech and FZJ-NO3 mechanisms (Table 2). The signal of the VOCUS PTR-MS instrument at the mass of $ISOPCNO_3$ confirms also the low reaction rate constants with OH determined experimentally in Lee et al. (2014b).

HPALD formation from the reaction of isoprene with NO_3 is only implemented in the FZJ-NO3 mechanism. Wolfe et al. (2012) investigated the photo-oxidation of a closely-related compound of HPALD to constrain photolysis rates and reaction rate constants in the reaction with OH (Reaction R36) and O_3 (Reaction R37). A fast OH-reaction rate constant $5.1 \times 10^{-11}\,s^{-1}cm^3$ was found. This value is implemented in the MCM, Caltech and FZJ-NO3 mechanisms (Table 2). The reaction rate constant of HPALD with ozone was determined in Wolfe et al. (2012) to be $1.2 \times 10^{-18}\,s^{-1}cm^3$ making the ozone reaction irrelevant for typical atmospheric conditions. There are no experimental values for the reaction rate constant of HPALD with NO_3. Structure activity relationship (SAR) described in Kerdouci et al. (2014) cannot be applied because the effect of a COOH substituent in the β-position of the C=C double at which NO_3 adds is not considered. Omitting this substituent results in a reaction rate constant similar to the value in the MCM, indicating that a COOH substituent further lowers the reaction rate constant.

In the MCM, a fast reaction rate constant of HPALD with ozone (Reaction R37) is implemented, which would lead to a short chemical lifetime of $4.6\,h$ for conditions of the experiment in this work (100 ppbv O_3). In addition, the MCM assumes

that HPALD reacts with NO_3 (Reaction R38) with a fast reaction rate constant of $1.2 \times 10^{-14}\,s^{-1}cm^3$, which would lead to a significant loss of HPALD in the last part of the experiment on 13 August 2018 (Experiment #4). This is inconsistent with the temporal behaviour of the signal observed by the VOCUS PTR-MS instrument, which is explained by the loss of HPALD by only its reaction with OH (Fig. 5, Panel (c)). In the experiments on 09 August 2018 (Experiment #1), when OH reactions were suppressed by the presence of the OH scavenger, the temporal behaviour of the HPALD signal is fully consistent with only the loss due to dilution (Fig. 4, Panel (c)).

The further oxidation of epoxides produced from ring-closure reactions of nitrate alkoxy radicals calculated in Vereecken et al. (2021) have not been investigated so far. The temporal behaviour of signals measured by the VOCUS PTR-MS instrument suggests that their loss rate can be explained by only the dilution rate in the experiments indicating that chemical loss was not significant even in the presence of several $100\,pptv$ NO_3, $100\,ppbv$ O_3 and presumably several 10^5 OH in the last period of the experiment on 13 August 2018 (Experiment #4) (Fig. 5, Panel (j)). An upper limit value of the reaction rate constant of the reaction of epoxides with OH of $1.2 \times 10^{-11}\,s^{-1}cm^3$ ($T = 298\,K$) can be assumed similar to the value found for epoxides produced from the reaction of OH reaction of hydroperoxides derived from isoprene (Bates et al., 2014) making chemical loss a minor loss pathway for typical conditions during night-time.

In the presence of aerosol surface, epoxides could be lost by particle uptake, but this was not relevant in the experiments analysed in this work due to the absence of seed aerosol. Loss to the Teflon surface of the chamber was not significant as demonstrated by the consistency of the loss rate with the dilution rate in the experiments.

5.8   OH and NO_3 reactivity from products

Overall, night-time oxidation of products from the reaction of isoprene with NO_3 appear to be of minor importance. This is further supported by measurements of total OH and NO_3 reactivity in the experiments in this work. In Figure 9, measured OH reactivity from organic compounds (Section 2.1) is compared to values calculated from modelled concentrations of products for the experiment on 13 August 2013 (Experiment #4), when the total consumption of isoprene by NO_3 was highest. Reaction rate constants for the reactions of organic compounds with OH are applied from the FZJ-NO3 mechanism.

OH reactivity is dominated by isoprene right after each injection (Fig. 9). After isoprene has reacted away, OH reactivity is only approximately 30 % of the initial reactivity demonstrating the much lower reactivity from products than from isoprene. The major organic nitrate and epoxides produced from the reaction of NO_3 with isoprene explain approximately 50 % of the total reactivity of organic products. Hydroperoxy aldehydes (HPALD), which are partly also produced from the OH oxidation of isoprene, contribute approximately 15 % to the OH reactivity from products. A similar contribution is obtained from compounds that are formed from the oxidation of isoprene by OH and O_3, ISOPOOH, HCHO, MVK and MACR. At the end of the experiment, 25 % of the total reactivity is due to a high number of organic compounds that are produced from minor reaction pathways or secondary oxidation.

The good agreement in the temporal behaviour of the observed and calculated OH reactivity is consistent with the low loss rate of products due to further oxidation reactions. In addition, measured OH reactivity values are consistent with OH reaction rate constants implemented in the FZJ-NO3 mechanism, so that further OH oxidation of products is small for night-
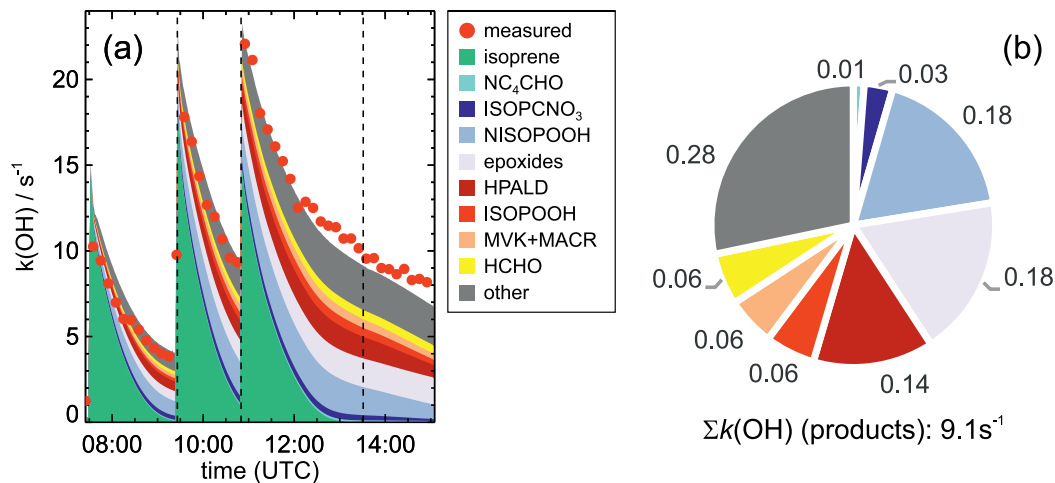
Figure 9. Comparison of measured OH reactivity from organic compounds and OH reactivity (left panel) calculated from concentrations of organic compounds modelled applying the FZJ-NO3 chemical mechanism for the experiment on 13 August 2018 (Experiment #4). The reactivity from hydroperoxide compounds (NISOPOOH, ISOPOOH) is partly invisible for the LP-LIF instrument, because these species produce OH radicals after reacting with it. The OH yield is rather uncertain, but is expected to be less than 10 % for example in the Caltech mechanism. In addition, the relative distribution of OH reactivity from organic products is shown (right panel). OH reactivity from organic compounds is derived by subtracting the reactivity from NO_2 and O_3 calculated from measured concentrations from the measured total OH reactivity. "Other" compounds include a high number of organic compounds that are produced in the reaction of isoprene with OH, O_3 and NO_3 and for which loss by the reaction with OH is implemented in the FZJ-NO3 mechanism. Dashed vertical lines indicate times, when isoprene, NO_2 and O_3 were re-injected. The last injection included only NO_2 and O_3.

670 time conditions, when OH concentrations are typically maximum a few 10^5 cm^3 (Stone et al., 2012, 2014; Lu et al., 2014; Tan et al., 2017).

OH oxidation of nitrate hydroperoxides is most important due to their fast reaction rate constant and their high concentrations for typical night-time conditions, when HO_2 + RO_2 reactions can dominate the loss of RO_2. However, part of the reactivity from hydroperoxides is invisible for the OH reactivity instrument, because OH is partly produced in their reactions with OH.

675 Approximately 90 % of the reactivity is detected assuming an OH yield of 10 % as implemented in the Caltech and FZJ-NO3 mechanisms. In contrast, an OH yield of 100 % is assumed for NISOPOOH in the MCM, which is likely too high as formation of epoxide products is expected to be a major reaction pathway.

OH oxidation of HPALD produced from unimolecular reactions of nitrate RO_2 can be significant because of the fast reaction of HPALD with OH.

680 In contrast the absolute values of OH reactivity as well as its temporal behaviour calculated from model calculations using the MCM with high OH reaction rate constants and high yields of NISOPOOH and NC_4CHO leads to results that are inconsistent with the observed OH reactivity (Fig. A12). This confirms that the MCM does not reproduce the product distribution and loss rates of products.

Dewald et al. (2020) discussed the NO_3 reactivity measured in the experiments also investigated in this work. Consistent with conclusions above that the chemical loss of products by NO_3 was not relevant, the authors found that the NO_3 reactivity could be fully explained by the reactivity from isoprene and propene in these experiments. This confirms that loss of organic products from the reaction of isoprene with NO_3 due to further NO_3 oxidation is small compared to the dilution rate in the chamber experiments.

6   Comparison to previous experiments

The high yield of MVK and MACR from the decomposition of β-RO radicals in the Caltech mechansim was derived from chamber experiments in Schwantes et al. (2015). In their experiments, 54 to 74 % of the nitrate RO_2 reacted with HO_2, so that the majority of alkoxy radicals was formed from this reaction. MVK and MACR concentrations, however, were only measured in 2 experiments in Schwantes et al. (2015), one of which was used to determine the MVK and MACR yields from the reaction of HO_2 + RO_2. The overall yield of the sum of MVK and MACR was relatively low with a value of approximately 15 %. In order to determine the yield of MVK and MACR from the decomposition of alkoxy radicals from the RO_2 + HO_2 reactions, production from the isoprene oxidation by OH and O_3 and from the potential decomposition of alkoxy radicals produced from other reaction channels needed to be subtracted. The authors used model calculations to estimate the actual OH concentration. Uncertainties in this calculations may explain the high MVK and MACR yield in Schwantes et al. (2015).

MVK and MACR concentrations were also measured in an experiment in the SAPHIR chamber reported by Rollins et al. (2009), in which low reactant concentrations were present as in this work (10 ppbv isoprene, 20 to 30 ppbv NO_2, 40 to 60 ppbv O_3). According to model calculations in Rollins et al. (2009) using the MCM 3.2, the fate of nitrate RO_2 radicals from isoprene with NO_3 was dominated by their reactions with HO_2. Measured MVK and MACR concentrations were consistent with the production of MVK and MACR mainly from the ozonolysis of isoprene. Therefore, this result supports that MVK and MACR are not produced from the decomposition of alkoxy radicals from β-RO_2 radicals. This is further supported by other experiments investigating the reaction of isoprene with NO_3 at high reactant concentrations (Barnes et al., 1990; Kwok et al., 1996; Perring et al., 2009) and also in chamber experiments of Kwan et al. (2012).

Similar to the experiments in this work, products that have the sum formulas of nitrate epoxide products expected to be formed in the FZJ-NO3 mechanism were observed in the experiments in Kwan et al. (2012) and Schwantes et al. (2015): (1) $C_5H_9NO_5$ compounds, which appear at the same mass as NISOPOOH, (2) $C_5H_7NO_5$ compounds from epoxy-RO_2 + RO_2 reactions, (3) $C_5H_9NO_6$ compounds from epoxy-RO_2 + HO_2 reactions.

In Kwan et al. (2012) and Schwantes et al. (2015) it is suggested that the product with the sum formula $C_5H_9NO_6$ is a hydroxy hydroperoxy nitrate and that the product with the sum formula $C_5H_7NO_5$ is a hydroxy carbonyl nitrate from a 1,5-H-shift reaction of δ nitrate alkoxy radicals. Vereecken et al. (2021) calculated a reaction rate of $2.2 \times 10^6 \, s^{-1}$ ($T = 298$ K), which makes the 1,5-H-shift reaction too low to compete with the ring-closure reaction forming epoxy alkyl radicals ($1.2 \times 10^8 \, s^{-1}$, $T = 298$ K) and subsequent O_2 addition. It is worth noting that compounds suggested by Kwan et al. (2012) and Schwantes et al. (2015) would only be produced from nitrate δ-RO_2 radicals that have small yields, whereas the nitrate epoxy products

in the FZJ-NO3 mechanism are also produced from the most abundant nitrate β-RO$_2$ radicals. This may also explain why compounds with these sum formulas were clearly detected in the experiments in all studies.

In the experiments in Kwan et al. (2012) and Schwantes et al. (2015), a $C_5H_8O_3$ compound without a nitrate functional group was observed, which is consistent with observations in this work. Because HPALD appears at the same mass and HPALD is also produced from OH oxidation, the authors concluded that $C_5H_8O_3$ is a product from the reaction of isoprene with OH. Nevertheless, their observations of $C_5H_8O_3$ compounds could also be partly due to the production of epoxy species from the oxidation of isoprene by NO$_3$ as described in the FZJ-NO3 mechanism.

The other product without a nitrate group that is produced from the ring-closure pathway of nitrate alkoxy radicals in the FZJ-NO3 mechanism, $C_5H_8O_4$, was not observed in the experiments in Kwan et al. (2012) and Schwantes et al. (2015). The reason could be that the chemical lifetime of RO$_2$ radicals was too short in the experiments in Kwan et al. (2012), in which high concentrations of reactants were present, so that the 1,6-H-shift reaction of the epoxy-RO$_2$ radical producing the $C_5H_8O_4$ compound could not compete with bimolecular reactions. Similarly, RO$_2$ reactions with HO$_2$ were favoured in the experiments in Schwantes et al. (2015), so that the 1,6-H reaction may have not been competitive.

Interestingly, similar to the experiments in this work, no organic nitrate with the sum formula $C_4H_5NO_4$ that is expected to be formed from the ring-closure reactions of nitrate alkoxy radicals (Fig. 6) was observed in the experiments in Kwan et al. (2012) and Schwantes et al. (2015). This further suggests that there is no significant production of this compound.

NISOPOOH has been detected by mass spectrometer instruments in previous chamber studies by Ng et al. (2008), Kwan et al. (2012) and Schwantes et al. (2015). Similar to this work, the instruments were not calibrated for NISOPOOH, but the sensitivity of the instrument was calibrated for nitrate alcohols (ISOPCNO$_3$). The sensitivity for other organic nitrates such as NISOPOOH was estimated from calculations of the dipole moment and polarisability (Ng et al., 2008; Kwan et al., 2012; Schwantes et al., 2015).

In the experiments of Schwantes et al. (2015), HO$_2$ concentrations were enhanced. NISOPOOH yields were between 0.32 and 0.41, when 54 and 76 % of the nitrate RO$_2$ were calculated to react with HO$_2$. The authors calculated that these yields are consistent with a 50 % branching ratio of the reaction of nitrate RO$_2$ with HO$_2$ (Reaction R2) to form alkoxy radicals. An uncertainty of ± 20 % of the measured NISOPOOH concentration is stated. The uncertainty of the alkoxy radical yield, however, could be higher because the calculation also requires the knowledge of the fraction of isoprene that reacted with NO$_3$ and the fraction of RO$_2$ that reacted with HO$_2$, both of which are uncertain because NO$_3$ and HO$_2$ concentrations were not measured. Therefore, a NISOPOOH yield of the reaction of nitrate RO$_2$ with HO$_2$ higher than 50 % may also be consistent with the experimental results in Schwantes et al. (2015).

Ng et al. (2008) quantified NISOPOOH concentrations in their chamber experiment, which was performed at high concentrations of reactants (800 ppbv isoprene, 120 ppbv N$_2$O$_5$). They determined that 50 % of the reacted isoprene resulted in the formation of NISOPOOH, but the fraction of nitrate RO$_2$ that reacted with HO$_2$ could not be determined to calculate yields from specific reactions. Therefore, their experiments cannot be used to derive information about potential alkoxy radical formation from the reaction of RO$_2$ with HO$_2$. HO$_2$ concentrations in experiments in Kwan et al. (2012) were presumably

small because high reactant concentrations were used. This explains the relatively small overall NISOPOOH formation of 10 % from the reaction of isoprene with NO_3.

Kwan et al. (2012) assumed that specific C_5 organic compounds (HPALD, ISOPOOH, C_5 hydroxy carbonyl $C_5H_8O_2$) and MVK and MACR, all of which were quantified in their chamber experiments, were exclusively formed from OH radicals that are formed as co-product of alkoxy radicals. In this case, the yield of nitrate alkoxy radical formation competing with the formation of NISOPOOH in the reaction of nitrate RO_2 with HO_2 is 38 to 58 %. Although the experiments were performed in the absence of ozone, so that OH was not produced by ozonolysis reactions, this approach gives only an upper limit of the yield because OH as well as some of the organic products may not have been exclusively produced by this assigned reaction pathway. For example, HPALD can also be produced from the oxidation of isoprene by NO_3 from 1,6-H reactions of nitrate RO_2 (Vereecken et al. (2021), Fig. 3, Section 5.6).

HPALD was also observed in chamber experiments in Kwan et al. (2012) and Schwantes et al. (2015). The authors attributed the observations to the OH oxidation of isoprene, but their observations could also indicate HPALD formation from nitrate RO_2. Specifically in the experiments in Schwantes et al. (2015) the total loss rate of nitrate RO_2 were calculated to be in the range of 0.03 to 0.13 s^{-1}, so that 1,6-H shift reactions with rates 0.02 and 0.05 s^{-1} ($T = 298$ K) calculated in Vereecken et al. (2021) can compete with bimolecular loss reactions.

Tsiligiannis et al. (2022) showed that a C_4 nitrate with the sum formula $C_4H_7NO_5$ was observed by the I^- CIMS instrument in the experiments in this work and also in several field campaigns, in which isoprene oxidation by NO_3 was important. This compound was also detected in the chamber experiments by the Br^- CIMS instrument (Wu et al., 2021), but signals observed by the VOCUS PTR-MS instrument at the respective mass were below the limit of detection. Yields of $C_4H_7NO_5$ determined in previous chamber experiments in Schwantes et al. (2015) were below 1 %.

Mayhew et al. (2022) applied the three chemical models investigated in this work to field observations in an urban location in Beijing in June 2017. Differences between model results were similar as calculated in this work. The comparison of modelled data with measurements, however, is more complex for field experiments than for chamber experiments, because trace gas concentrations are not only impacted by chemical process, but also by transport. In the field campaign in Beijing, organic nitrates from isoprene were detected by an I^- CIMS instrument. The instrument was not specifically calibrated for those compounds, but the same sensitivity as for isoprene epoxides (IEPOX) was assumed. In general, concentrations of measured isoprene-derived organic nitrates were lower than calculations for all three models in the night (Mayhew et al., 2022). As pointed out by the authors, the potential loss of epoxide nitrates due to particle uptake could not entirely explain the model-measurement discrepancies.

Overall, results in the experiments in this work appear to be consistent with results in previous experiments supporting the validity of the FZJ-NO3 mechanism.

7 Conclusions

The oxidation of isoprene by the nitrate radical, NO_3, was investigated in chamber experiments covering different atmospherically relevant chemical regimes. The chemical lifetimes of RO_2 radicals formed in the initial reaction of isoprene with NO_3 were in the range of atmospheric lifetimes with values between $30\,s$ and several minutes due to atmospheric concentrations of reaction partners (RO_2, HO_2 and NO_3). In one experiment, $RO_2 + HO_2$ reactions were favoured by producing HO_2 and OH radicals in the ozonolysis of propene in the presence of excess CO for the conversion of OH to HO_2 radicals. Results from calculations of three near-explicit chemical models (MCM, Caltech, FZJ-NO3) were compared to measurements.

A critical difference between the three chemical mechanisms is the fate of nitrate alkoxy radicals formed in the radical reaction chain which mainly undergo ring-closure reactions in the FZJ-NO3 mechanisms, whereas decomposition to MVK and MACR is not competitive. Measured concentrations of MVK and MACR in the experiments in this work are consistent with their production from only O_3 and OH reactions with isoprene in agreement with results in previous chamber experiments in Rollins et al. (2009) and Kwan et al. (2012).

Mass signals of most of the organic products expected from the ring-closure reactions of the nitrate alkoxy radicals were detected by the VOCUS PTR-MS instrument demonstrating that the reactions calculated in Vereecken et al. (2021) may indeed be relevant pathways. Signals at the same masses were observed by chemical ionization mass spectrometer in previous chamber experiments (Kwan et al., 2012; Schwantes et al., 2015). One product of the ring-closure reaction of nitrate alkoxy radicals, which has the sum formula $C_4H_5NO_4$, calculated by Vereecken et al. (2021) to be produced could not be detected by the VOCUS PTR-MS instrument in the experiments in this work and has also not been observed in experiments in Kwan et al. (2012) and Schwantes et al. (2015). Therefore, the reaction pathway leading to this product is likely less important than implemented in the FZJ-NO3 mechanism, but this is within the uncertainty of the calculations in Vereecken et al. (2021).

The formation of hydroperoxy aldehydes (HPALD) from 1,6-H-shift reactions of nitrate Z-δ-RO_2 isomers is only implemented in the FZJ-NO3 mechanism (Vereecken et al., 2021).

A clear signal at the mass of HPALD was detected by the VOCUS PTR-MS instrument in all experiments in this work. This was also the case in the experiment, when an OH scavenger was present (09 August 2018, Experiment #1), demonstrating that HPALD was formed from the reaction of isoprene with NO_3 and that the HPALD was not only formed from the small fraction of isoprene reacting with OH radicals and ozone in the experiments. This is also consistent with previous chamber experiments by Kwan et al. (2012) and Schwantes et al. (2015), in which HPALD formation was observed but attributed to the production from the reaction of OH with isoprene. Measurements of total organic nitrates in Brownwood et al. (2021) for the same experiments, however, give high yields of organic nitrates hinting that reaction rate constants of 1,6-H-shift reactions might be lower than calculated by Vereecken et al. (2021).

In the night, the fate of nitrate-RO_2 includes bimolecular reactions with HO_2 radicals, other RO_2 radicals and NO_3 radicals, all of which are significant for atmospheric conditions.

None of the current chemical models can predict $C_4H_7NO_5$ yields estimated in Tsiligiannis et al. (2022). They could be formed from further oxidation of first-generation C_5 nitrates by OH (Wennberg et al., 2018), but the expected yields in the

experiments in this work are small due to the low OH concentrations. In addition, $C_4H_7NO_5$ compounds were also detected in the experiment, when OH concentrations were suppressed by an OH scavenger demonstrating that they are also formed from other reaction pathways. Further investigations are required to quantify the importance of $C_4H_7NO_5$ in the NO_3 isoprene oxidation scheme.

820   In the nocturnal atmosphere, isoprene is not only oxidized by NO_3, but also a significant fraction reacts with ozone depending on the availability of nitrogen oxides and ozone (Edwards et al., 2017). It is worth noting that due to the fast reaction rate constant of isoprene with OH, reaction with OH could also contribute to the overall loss of isoprene in the night. Part of the OH radicals can be produced in the subsequent reaction chain of the NO_3 oxidation of isoprene (Kwan et al., 2012; Vereecken et al., 2021). Fast unimolecular reactions of RO_2 from the reaction of isoprene with OH (Peeters et al., 2014) can further

825   gain in importance during the night compared to daytime (Novelli et al., 2020) because of the long chemical lifetime of RO_2 radicals in the range of minutes in the absence of NO, which is often the most important reaction partner for RO_2 radicals during the day. Therefore, the yield of HPALD produced from the OH reactions with isoprene can be high in the night despite low OH concentrations. HPALD photolysis could then contribute to OH production on the next day (Wolfe et al., 2012).

Only a small fraction of first-generation organic products are further oxidized for atmospheric night-time conditions but are

830   most likely chemically processed by photolysis and reaction with OH on the next day. Reaction rate constants of the reactions of nitrate-carbonyl, nitrate-alcohol and epoxides with NO_3 and O_3 give chemical lifetimes which are longer than a night for typical concentrations of NO_3 and O_3. Also HPALD does not react efficiently with NO_3 and O_3. Reaction rate constants of these reactions as implemented in chemical models such as the MCM, which lead to short chemical lifetimes in the range of hours, need to be revised.

835   Overall, results from experiments in this work demonstrate that the FZJ-NO3 mechanism for isoprene (Vereecken et al., 2021) gives more complete and accurate description of the nocturnal oxidation of isoprene than previous chemical mechanisms. New reaction pathways in Vereecken et al. (2021) can have consequences for the nocturnal loss of reactive nitrogen and formation of secondary organic aerosol. However, large uncertainties still exist in the exact distribution of the different RO_2 isomers formed in the reaction of isoprene with NO_3 and their fate. Specifically, the yield of alkoxy radicals from the reaction

840   of nitrate-RO_2 with HO_2 is uncertain. Calibration of instruments detecting organic nitrate products for specific reaction pathways is urgently needed in future experiments in order to determine the absolute importance of these reaction pathways for atmospheric conditions.

Data availability. Data from the experiments in the SAPHIR chamber used in this work are available on the EUROCHAMP database webpage (https://data.eurochamp.org). Experiment on 09 August 2018 (Experiment #1): Fuchs et al. (2018a), experiment on 10 August 2018

845   (Experiment #2): Fuchs et al. (2018b), experiment on 12 August 2018 (Experiment #3): Fuchs et al. (2018c), experiment on 13 August 2018 (Experiment #4): Fuchs et al. (2018d).

Author contributions. PC and HF wrote the manuscript, analysed the data and did model calculations of the experiments. SB, MH, JF, AN and HF designed and executed the experiments. LV provided insights into the chemical mechanisms. LH, TH, SK, TM, RT, DR, FR, RW, BB, JF, ET, JC, PD, NS, JF, JS, FB were responsible for measurements used in this work. All authors intensively discussed the manuscript and thereby contributed to the writing.

Competing interests. The authors declare no competing interests.

Financial support. This research has been supported by the European Research Council (ERC), (SARLEP grant agreement no. 681529), European Commission (EC) under the European Union's Horizon 2020 research and innovation program, (Eurochamp 2020 grant agreement no. 730997 and FORCeS grant agreement no. 821205), Vetenskapsrådet (VR, grant nos. 2014-05332 and 2018-04430), and Svenska Forskningsrådet Formas (grant nos. 2015-1537 and 2019-586).

References

Albrecht, S. R., Novelli, A., Hofzumahaus, A., Kang, S., Baker, Y., Mentel, T., Wahner, A., and Fuchs, H.: Measurements of hydroperoxy radicals (HO_2) at atmospheric concentrations using bromide chemical ionisation mass spectrometry, Atmos. Meas. Tech., 12, 891–902, https://doi.org/10.5194/amt-12-891-2019, 2019.

860 Ashbourn, S. F. M., Jenkin, M. E., and Clemitshaw, K. C.: Laboratory studies of the response of a peroxy radical chemical amplifier to HO_2 and a series of organic peroxy radicals, J. Atmos. Chem., 29, 233–266, https://doi.org/10.1023/A:1005992316512, 1998.

Atkinson, R., Baulch, D. L., Cox, R. A., Crowley, J. N., Hampson, R. F., Hynes, R. G., Jenkin, M. E., Rossi, M. J., Troe, J., and Subcommittee, I.: Evaluated kinetic and photochemical data for atmospheric chemistry: Volume II - gas phase reactions of organic species, Atmos. Chem. Phys., 6, 3625–4055, https://doi.org/10.5194/acp-6-3625-2006, 2006.

865 Barnes, I., Bastian, V., Becker, K. H., and Tong, Z.: Kinetics and products of the reactions of nitrate radical with monoalkenes, dialkenes, and monoterpenes, J. Phys. Chem., 94, 2413–2419, https://doi.org/10.1021/j100369a041, 1990.

Bates, K. H. and Wennberg, P.: Isoprene oxidation model (Version 5), CaltechDATA [Data set], https://doi.org/10.22002/D1.247, 2017.

Bates, K. H., Crounse, J. D., Clair, J. M. S., Bennett, N. B., Nguyen, T. B., Seinfeld, J. H., Stoltz, B. M., and Wennberg, P. O.: Gas phase production and loss of isoprene epoxydiols, J. Phys. Chem. A, 118, 1237-1246, https://doi.org/10.1021/jp4107958, 2014.

870 Berndt, T., Hyttinen, N., Herrmann, H., and Hansel, A.: First oxidation products from the reaction of hydroxyl radicals with isoprene for pristine environmental conditions, Com. Chem., 2, 21, https://doi.org/10.1038/s42004-019-0120-9, 2019.

Bohn, B. and Zilken, H.: Model-aided radiometric determination of photolysis frequencies in a sunlit atmosphere simulation chamber, Atmos. Chem. Phys., 5, 191–206, https://doi.org/10.5194/acp-5-191-2005, 2005.

Brown, S. S., Gouw, J. A., d., Warneke, C., Ryerson, T. B., Dubé, W. P., Atlas, E., Weber, R. J., Peltier, R. E., Neuman, J. A., Roberts, J. M., 875 Swanson, A., Flocke, F., McKeen, S. A., Brioude, J., Sommariva, R., Trainer, M., Fehsenfeld, F. C., and Ravishankara, A. R.: Nocturnal isoprene oxidation over the Northeast United States in summer and its impact on reactive nitrogen partitioning and secondary organic aerosol, Atmos. Chem. Phys., 9, 3027–3042, https://doi.org/10.5194/acp-9-3027-2009, 2009.

Brownwood, B., Turdziladze, A., Hohaus, T., Wu, R., Mentel, T. F., Carlsson, P. T. M., Tsiligiannis, E., Hallquist, M., Andres, S., Hantschke, L., Reimer, D., Rohrer, F., Tillmann, R., Winter, B., Liebmann, J., Brown, S. S., Kiendler-Scharr, A., Novelli, A., Fuchs, H., and Fry, 880 J. L.: Gas-particle partitioning and SOA yields of organonitrate products from NO_3-initiated oxidation of isoprene under varied chemical regimes, Earth Space Chem., 5, 785–800, https://doi.org/10.1021/acsearthspacechem.0c00311, 2021.

Canosa-Mas, C. E., Smith, S. J., Waygood, S. J., and Wayne, R. P.: Study of the temperature dependence of the reaction of the nitrate radical with propene, J. Chem. Soc. Farad. Trans., 87, 3473–3478, https://doi.org/10.1039/FT9918703473, 1991.

Cho, C., Hofzumahaus, A., Fuchs, H., Dorn, H. P., Glowania, M., Holland, F., Rohrer, F., Vardhan, V., Kiendler-Scharr, A., Wahner, A., and 885 Novelli, A.: Characterization of a chemical modulation reactor (CMR) for the measurement of atmospheric concentrations of hydroxyl radicals with a laser-induced fluorescence instrument, Atmos. Meas. Tech., 14, 1851–1877, https://doi.org/10.5194/amt-14-1851-2021, 2021.

Crounse, J. D., Paulot, F., Kjaergaard, H. G., and Wennberg, P. O.: Peroxy radical isomerization in the oxidation of isoprene, Phys. Chem. Chem. Phys., 13, 13 607–13 613, https://doi.org/10.1039/C1CP21330J, 2011.

890 Dewald, P., Liebmann, J. M., Friedrich, N., Shenolikar, J., Schuladen, J., Rohrer, F., Reimer, D., Tillmann, R., Novelli, A., Cho, C., Xu, K., Holzinger, R., Bernard, F., Zhou, L., Mellouki, W., Brown, S. S., Fuchs, H., Lelieveld, J., and Crowley, J. N.: Evolution of NO_3 reactivity during the oxidation of isoprene, Atmos. Chem. Phys., 20, 10 459–10 475, https://doi.org/10.5194/acp-20-10459-2020, 2020.

Edwards, P. M., Aikin, K. C., Dube, W. P., Fry, J. L., Gilman, J. B., de Gouw, J. A., Graus, M. G., Hanisco, T. F., Holloway, J., Hübler, G., Kaiser, J., Keutsch, F. N., Lerner, B. M., Neuman, J. A., Parrish, D. D., Peischl, J., Pollack, I. B., Ravishankara, A. R., Roberts, J. M.,

895   Ryerson, T. B., Trainer, M., Veres, P. R., Wolfe, G. M., Warneke, C., and Brown, S. S.: Transition from high- to low-NO_x control of night-time oxidation in the southeastern US, Nature Geosci., 10, 490, https://doi.org/10.1038/ngeo2976, 2017.

Fuchs, H., Bohn, B., Hofzumahaus, A., Holland, F., Lu, K. D., Nehr, S., Rohrer, F., and Wahner, A.: Detection of HO_2 by laser-induced fluorescence: calibration and interferences from RO_2 radicals, Atmos. Meas. Tech., 4, 1209–1255, https://doi.org/10.5194/amt-4-1209-2011, 2011.

900   Fuchs, H., Dorn, H. P., Bachner, M., Bohn, B., Brauers, T., Gomm, S., Hofzumahaus, A., Holland, F., Nehr, S., Rohrer, F., Tillmann, R., and Wahner, A.: Comparison of OH concentration measurements by DOAS and LIF during SAPHIR chamber experiments at high OH reactivity and low NO concentration, Atmos. Meas. Tech., 5, 1611–1626, https://doi.org/10.5194/amt-5-1611-2012, 2012.

Fuchs, H., Hofzumahaus, A., Rohrer, F., Bohn, B., Brauers, T., Dorn, H.-P., Häseler, R., Holland, F., Kaminski, M., Li, X., Lu, K., Nehr, S., Tillmann, R., Wegener, R., and Wahner, A.: Experimental evidence for efficient hydroxyl radical regeneration in isoprene oxidation,

905   Nature Geosci., 6, 1023–1026, https://doi.org/10.1038/NGEO1964, 2013.

Fuchs, H., Novelli, A., Rolletter, M., Hofzumahaus, A., Pfannerstill, E. Y., Kessel, S., Edtbauer, A., Williams, J., Michoud, V., Dusanter, S., Locoge, N., Zannoni, N., Gros, V., Truong, F., Sarda-Esteve, R., Cryer, D. R., Brumby, C. A., Whalley, L. K., Stone, D., Seakins, P. W., Heard, D. E., Schoemaecker, C., Blocquet, M., Coudert, S., Batut, S., Fittschen, C., Thames, A. B., Brune, W. H., Ernest, C., Harder, H., Muller, J. B. A., Elste, T., Kubistin, D., Andres, S., Bohn, B., Hohaus, T., Holland, F., Li, X., Rohrer, F., Kiendler-Scharr, A., Tillmann,

910   R., Wegener, R., Yu, Z., Zou, Q., and Wahner, A.: Comparison of OH reactivity measurements in the atmospheric simulation chamber SAPHIR, Atmos. Meas. Tech., 10, 4023–4053, https://doi.org/10.5194/amt-10-4023-2017, 2017.

Fuchs, H., Novelli, A., Cho, C., Rohrer, F., Tillmann, R., Reimer, D., Hohaus, T., Turdziladze, A., Dewald, P., Liebmann, J., Friedrich, N., Shenolikar, J., Schuladen, J., Crowley, J., Brown, S. S., Bernard, F., Zhou, L., Mentel, T., Wu, R., and Hamilton, J. F.: Atmospheric simulation chamber study: isoprene + NO_3 - Gas-phase oxidation - product study, AERIS [Data set], https://doi.org/10.25326/PZ5Q-9X18,

915   2018a.

Fuchs, H., Novelli, A., Cho, C., Rohrer, F., Tillmann, R., Reimer, D., Hohaus, T., Turdziladze, A., Dewald, P., Liebmann, J., Friedrich, N., Shenolikar, J., Schuladen, J., Crowley, J., Brown, S. S., Bernard, F., Zhou, L., Mentel, T., Wu, R., and Hamilton, J. F.: Atmospheric simulation chamber study: isoprene + NO_3 - Gas-phase oxidation - product study, AERIS [Data set], https://doi.org/10.25326/YZHF-T659, 2018b.

920   Fuchs, H., Novelli, A., Cho, C., Rohrer, F., Tillmann, R., Reimer, D., Hohaus, T., Turdziladze, A., Dewald, P., Liebmann, J., Friedrich, N., Shenolikar, J., Schuladen, J., Crowley, J., Brown, S. S., Bernard, F., Zhou, L., Mentel, T., Wu, R., and Hamilton, J. F.: Atmospheric simulation chamber study: isoprene + NO_3 - Gas-phase oxidation - product study, AERIS [Data set], https://doi.org/10.25326/JCST-0Y45, 2018c.

Fuchs, H., Novelli, A., Cho, C., Rohrer, F., Tillmann, R., Reimer, D., Hohaus, T., Turdziladze, A., Dewald, P., Liebmann, J., Friedrich,

925   N., Shenolikar, J., Schuladen, J., Crowley, J., Brown, S. S., Bernard, F., Zhou, L., Mentel, T., Wu, R., and Hamilton, J. F.: Atmospheric simulation chamber study: isoprene + NO_3 - Gas-phase oxidation - product study, AERIS [Data set], https://doi.org/10.25326/JCST-0Y45, 2018d.

Guenther, A. B., Jiang, X., Heald, C. L., Sakulyanontvittaya, T., Duhl, T., Emmons, L. K., and Wang, X.: The model of emissions of gases and aerosols from nature version 2.1 (MEGAN2.1): an extended and updated framework for modeling biogenic emissions, Geosci. Model

930   Dev., 5, 1471–1492, https://doi.org/10.5194/gmd-5-1471-2012, 2012.

Hantschke, L., Novelli, A., Bohn, B., Cho, C., Reimer, D., Rohrer, F., Tillmann, R., Glowania, M., Hofzumahaus, A., Kiendler-Scharr, A., Wahner, A., and Fuchs, H.: Atmospheric photooxidation and ozonolysis of Δ^3-carene and 3-caronaldehyde: rate constants and product yields, Atmos. Chem. Phys., 21, 12 665–12 685, https://doi.org/10.5194/acp-21-12665-2021, 2021.

Jenkin, M. E., Saunders, S. M., and Pilling, M. J.: The tropospheric degradation of volatile organic compounds: A protocol for mechanism development, Atmos. Environ., 31, 81–104, https://doi.org/10.1016/S1352-2310(96)00105-7, 1997.

Jenkin, M. E., Young, J. C., and Rickard, A. R.: The MCM v3.3.1 degradation scheme for isoprene, Atmos. Chem. Phys., 15, 11 433–11 459, https://doi.org/10.5194/acp-15-11433-2015, 2015.

Jenkin, M. E., Valorso, R., Aumont, B., and Rickard, A. R.: Estimation of rate coefficients and branching ratios for reactions of organic peroxy radicals for use in automated mechanism construction, Atmos. Chem. Phys., 19, 7691–7717, https://doi.org/10.5194/acp-19-7691-2019, 2019.

Keehan, N. I., Brownwood, B., Marsavin, A., Day, D. A., and Fry, J. L.: A thermal-dissociation–cavity ring-down spectrometer (TD-CRDS) for the detection of organic nitrates in gas and particle phases, Atmos. Meas. Tech., 13, 6255–6269, https://doi.org/10.5194/amt-13-6255-2020, 2020.

Kerdouci, J., Picquet-Varrault, B., and Doussin, J.-F.: Structure–activity relationship for the gas-phase reactions of NO_3 radical with organic compounds: Update and extension to aldehydes, Atmos. Environ., 84, 363–372, https://doi.org/10.1016/j.atmosenv.2013.11.024, 2014.

Krechmer, J., Lopez-Hilfiker, F., Koss, A., Hutterli, M., Stoermer, C., Deming, B., Kimmel, J., Warneke, C., Holzinger, R., Jayne, J., Worsnop, D., Fuhrer, K., Gonin, M., and de Gouw, J.: Evaluation of a new reagent-ion source and focusing ion–molecule reactor for use in proton-transfer-reaction mass spectrometry, Anal. Chem., 90, 12 011–12 018, https://doi.org/10.1021/acs.analchem.8b02641, 2018.

Kwan, A. J., Chan, A. W. H., Ng, N. L., Kjaergaard, H. G., Seinfeld, J. H., and Wennberg, P. O.: Peroxy radical chemistry and OH radical production during the NO_3-initiated oxidation of isoprene, Atmos. Chem. Phys., 12, 7499–7515, https://doi.org/10.5194/acp-12-7499-2012, 2012.

Kwok, E. S. C., Aschmann, S. M., Arey, J., and Atkinson, R.: Product formation from the reaction of the NO_3 radical with isoprene and rate constants for the reactions of methacrolein and methyl vinyl ketone with the NO_3 radical, Int. J. Chem. Kin., 28, 925–934, 1996.

Lee, B. H., Lopez-Hilfiker, F. D., Mohr, C., Kurtén, T., Worsnop, D. R., and Thornton, J. A.: An iodide-adduct high-resolution time-of-flight chemical-ionization mass spectrometer: Application to atmospheric inorganic and organic compounds, Environ Sci. Technol., 48, 6309–6317, https://doi.org/10.1021/es500362a, 2014a.

Lee, L., Teng, A. P., Wennberg, P. O., Crounse, J. D., and Cohen, R. C.: On rates and mechanisms of OH and O_3 reactions with isoprene-derived hydroxy nitrates, J. Phys. Chem. A, 118, 1622–1637, https://doi.org/10.1021/jp4107603, 2014b.

Lelieveld, J., Butler, T. M., Crowley, J. N., Dillon, T. J., Fischer, H., Ganzeveld, L., Harder, H., Lawrence, M. G., Martinez, M., Taraborrelli, D., and Williams, J.: Atmospheric oxidation capacity sustained by a tropical forest, Nature, 452, 737–740, https://doi.org/10.1038/nature06870, 2008.

Li, H., Almeida, T. G., Luo, Y., Zhao, J., Palm, B. B., Daub, C. D., Huang, W., Mohr, C., Krechmer, J. E., Kurtén, T., and Ehn, M.: Fragmentation inside proton-transfer-reaction-based mass spectrometers limits the detection of ROOR and ROOH peroxides, Atmos. Meas. Tech., 15, 1811–1827, https://doi.org/10.5194/amt-15-1811-2022, 2022.

Liebmann, J. M., Schuster, G., Schuladen, J. B., Sobanski, N., Lelieveld, J., and Crowley, J. N.: Measurement of ambient NO_3 reactivity: design, characterization and first deployment of a new instrument, Atmos. Meas. Tech., 10, 1241–1258, https://doi.org/10.5194/amt-10-1241-2017, 2017.
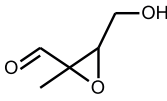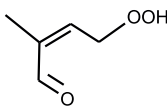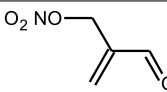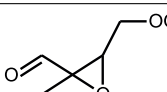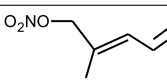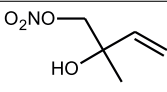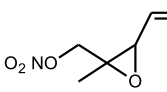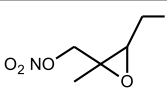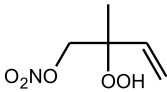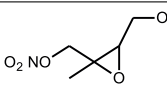
Liebmann, J. M., Muller, J. B. A., Kubistin, D., Claude, A., Holla, R., Plass-Dülmer, C., Lelieveld, J., and Crowley, J. N.: Direct measurements of NO_3 reactivity in and above the boundary layer of a mountaintop site: identification of reactive trace gases and comparison with OH

970   reactivity, Atmos. Chem. Phys., 18, 12 045–12 059, https://doi.org/10.5194/acp-18-12045-2018, 2018.

Lu, K. D., Rohrer, F., Holland, F., Fuchs, H., Brauers, T., Oebel, A., Dlugi, R., Hu, M., Li, X., Lou, S. R., Shao, M., Zhu, T., Wahner, A., Zhang, Y. H., and Hofzumahaus, A.: Nighttime observation and chemistry of HO_X in the Pearl River Delta and Beijing in summer 2006, Atmos. Chem. Phys., 14, 4979–4999, https://doi.org/10.5194/acp-14-4979-2014, 2014.

Mayhew, A. W., Lee, B. H., Thornton, J. A., Bannan, T. J., Brean, J., Hopkins, J. R., Lee, J. D., Nelson, B. S., Percival, C., Rickard, A. R.,

975   Shaw, M. D., Edwards, P. M., and Hamilton, J. F.: Evaluation of isoprene nitrate chemistry in detailed chemical mechanisms, Atmos. Chem. Phys., 22, 14 783–14 798, https://doi.org/10.5194/acp-22-14783-2022, 2022.

Mellouki, A., Ammann, M., Cox, R. A., Crowley, J. N., Herrmann, H., Jenkin, M. E., McNeill, V. F., Troe, J., and Wallington, T. J.: Evaluated kinetic and photochemical data for atmospheric chemistry: volume VIII – gas-phase reactions of organic species with four, or more, carbon atoms ($\geq$ C4), Atmos. Chem. Phys., 21, 4797–4808, https://doi.org/10.5194/acp-21-4797-2021, 2021.

980   Ng, N. L., Kwan, A. J., Surratt, J. D., Chan, A. W. H., Chhabra, P. S., Sorooshian, A., Pye, H. O. T., Crounse, J. D., Wennberg, P. O., Flagan, R. C., and Seinfeld, J. H.: Secondary organic aerosol (SOA) formation from reaction of isoprene with nitrate radicals (NO_3), Atmos. Chem. Phys., 8, 4117–4140, https://doi.org/10.5194/acp-8-4117-2008, 2008.

Nguyen, T. B., Tyndall, G. S., Crounse, J. D., Teng, A. P., Bates, K. H., Schwantes, R. H., Coggon, M. M., Zhang, L., Feiner, P., Milller, D. O., Skog, K. M., Rivera-Rios, J. C., Dorris, M., Olson, K. F., Koss, A., Wild, R. J., Brown, S. S., Goldstein, A. H., de Gouw, J. A., Brune,

985   W. H., Keutsch, F. N., Seinfeld, J. H., and Wennberg, P. O.: Atmospheric fates of Criegee intermediates in the ozonolysis of isoprene, Phys. Chem. Chem. Phys., 18, 10 241–10 254, https://doi.org/10.1039/C6CP00053C, 2016.

Novelli, A., Vereecken, L., Bohn, B., Dorn, H. P., Gkatzelis, G. I., Hofzumahaus, A., Holland, F., Reimer, D., Rohrer, F., Rosanka, S., Taraborrelli, D., Tillmann, R., Wegener, R., Yu, Z., Kiendler-Scharr, A., Wahner, A., and Fuchs, H.: Importance of isomerization reactions for OH radical regeneration from the photo-oxidation of isoprene investigated in the atmospheric simulation chamber SAPHIR, Atmos.

990   Chem. Phys., 20, 3333–3355, https://doi.org/10.5194/acp-20-3333-2020, 2020.

Novelli, A., Cho, C., Fuchs, H., Hofzumahaus, A., Rohrer, F., Tillmann, R., Kiendler-Scharr, A., Wahner, A., and Vereecken, L.: Experimental and theoretical study on the impact of a nitrate group on the chemistry of alkoxy radicals, Phys. Chem. Chem. Phys., https://doi.org/10.1039/D0CP05555G, 2021.

Paulot, F., Crounse, J. D., Kjaergaard, H. G., Kurten, A., St. Clair, J. M., Seinfeld, J. H., and Wennberg, P. O.: Unexpected epoxide formation

995   in the gas-phase photooxidation of isoprene, Science, 325, 730–733, https://doi.org/10.1126/science.1172910, 2009.

Peeters, J., Nguyen, T. L., and Vereecken, L.: HO_X radical regeneration in the oxidation of isoprene, Phys. Chem. Chem. Phys., 11, 5935–5939, https://doi.org/10.1039/b908511d, 2009.

Peeters, J., Müller, J.-F., Stavrakou, T., and Nguyen, V. S.: Hydroxyl radical recycling in isoprene oxidation driven by hydrogen bonding and hydrogen tunneling: The upgraded LIM1 mechanism, J. Phys. Chem. A, 118, 8625–8643, https://doi.org/10.1021/jp5033146, 2014.

1000   Perring, A. E., Wisthaler, A., Graus, M., Wooldridge, P. J., Lockwood, A. L., Mielke, L. H., Shepson, P. B., Hansel, A., and Cohen, R. C.: A product study of the isoprene+NO_3 reaction, Atmos. Chem. Phys., 9, 4945–4956, https://doi.org/10.5194/acp-9-4945-2009, 2009.

Robinson, M. A., Neuman, J. A., Huey, L. G., Roberts, J. M., Brown, S. S., and Veres, P. R.: Temperature dependent sensitivity of iodide chemical ionization mass spectrometers, EGUsphere, 2022, 1–17, https://doi.org/10.5194/amt-2022-295, 2022.

Rohrer, F., Bohn, B., Brauers, T., Brüning, D., Johnen, F.-J., Wahner, A., and Kleffmann, J.: Characterisation of the photolytic HONO-source

1005   in the atmosphere simulation chamber SAPHIR, Atmos. Chem. Phys., 5, 2189–2201, https://doi.org/10.5194/acp-5-2189-2005, 2005.

Rollins, A. W., Kiendler-Scharr, A., Fry, J. L., Brauers, T., Brown, S. S., Dorn, H. P., Dubé, W. P., Fuchs, H., Mensah, A., Mentel, T. F., Rohrer, F., Tillmann, R., Wegener, R., Wooldridge, P. J., and Cohen, R. C.: Isoprene oxidation by nitrate radical: alkyl nitrate and secondary organic aerosol yields, Atmos. Chem. Phys., 9, 6685–6703, https://doi.org/10.5194/acp-9-6685-2009, 2009.

Saunders, S. M., Jenkin, M. E., Derwent, R. G., and Pilling, M. J.: Protocol for the development of the Master Chemical Mechanism, MCMv3 (Part A): Tropospheric degradation of non-aromatic volatile organic compounds, Atmos. Chem. Phys., 3, 161–180, https://doi.org/10.5194/acp-3-161-2003, 2003.

Schwantes, R. H., Teng, A. P., Nguyen, T. B., Coggon, M. M., Crounse, J. D., St. Clair, J. M., Zhang, X., Schilling, K. A., Seinfeld, J. H., and Wennberg, P. O.: Isoprene NO_3 oxidation products from the RO_2 + HO_2 pathway, J. Phys. Chem. A, 119, 10 158–10 171, https://doi.org/10.1021/acs.jpca.5b06355, 2015.

Sobanski, N., Schuladen, J., Schuster, G., Lelieveld, J., and Crowley, J.: A 5-channel cavity ring-down spectrometer for the detection of NO_2, NO_3, N_2O_5, total peroxy nitrates and total alkyl nitrates, Atmos. Meas. Tech. Discuss., 2016, 1–32, https://doi.org/10.5194/amt-2016-191, 2016.

Stone, D., Whalley, L. K., and Heard, D. E.: Tropospheric OH and HO_2 radicals: field measurements and model comparisons, Chem. Soc. Rev., 41, 6348–6404, https://doi.org/10.1039/C2CS35140D, 2012.

Stone, D., Evans, M. J., Walker, H., Ingham, T., Vaughan, S., Ouyang, B., Kennedy, O. J., McLeod, M. W., Jones, R. L., Hopkins, J., Punjabi, S., Lidster, R., Hamilton, J. F., Lee, J. D., Lewis, A. C., Carpenter, L. J., Forster, G., Oram, D. E., Reeves, C. E., Bauguitte, S., Morgan, W., Coe, H., Aruffo, E., Dari-Salisburgo, C., Giammaria, F., Di Carlo, P., and Heard, D. E.: Radical chemistry at night: comparisons between observed and modelled HO_x, NO_3 and N_2O_5 during the RONOCO project, Atmos. Chem. Phys., 14, 1299–1321, https://doi.org/10.5194/acp-14-1299-2014, 2014.

Tan, Z., Fuchs, H., Lu, K., Hofzumahaus, A., Bohn, B., Broch, S., Dong, H., Gomm, S., Häseler, R., He, L., Holland, F., Li, X., Liu, Y., Lu, S., Rohrer, F., Shao, M., Wang, B., Wang, M., Wu, Y., Zeng, L., Zhang, Y., Wahner, A., and Zhang, Y.: Radical chemistry at a rural site (Wangdu) in the North China Plain: observation and model calculations of OH, HO_2 and RO_2 radicals, Atmos. Chem. Phys., 17, 663–690, https://doi.org/10.5194/acp-17-663-2017, 2017.

Tan, Z., Hantschke, L., Kaminski, M., Acir, I. H., Bohn, B., Cho, C., Dorn, H. P., Li, X., Novelli, A., Nehr, S., Rohrer, F., Tillmann, R., Wegener, R., Hofzumahaus, A., Kiendler-Scharr, A., Wahner, A., and Fuchs, H.: Atmospheric photo-oxidation of myrcene: OH reaction rate constant, gas-phase oxidation products and radical budgets, Atmos. Chem. Phys., 21, 16 067–16 091, https://doi.org/10.5194/acp-21-16067-2021, 2021.

Tsiligiannis, E., Wu, R., Lee, B. H., Salvador, C. M. G., Priestley, M., Carlsson, P. T. M., Novelli, S. K. A., Vereecken, L., Fuchs, H., Mayhew, A. W., Hamilton, J. F., Edwards, P. M., Fry, J. L., Brownwood, B., Brown, S. S., Wild, R. J., Bannan, T. J., Coe, H., Allan, J., Surrat, J. D., Bacak, A., Artaxo, P., Percival, C., Guo, S., Hu, M., Wang, T., Mentel, T. F., Thornton, J. A., and Hallquist, M.: A four carbon organonitrate as a significant product of secondary isoprene chemistry, Geophys. Res. Lett., 49, e2021GL097 366, https://doi.org/10.1029/2021GL097366, 2022.

Vereecken, L.: Replication Data for: Comparison of isoprene chemical mechanisms at atmospheric night-time conditions in chamber experiments: Evidence of hydroperoxy aldehydes and epoxy products from NO_3 oxidation, Jülich Data [Data set], https://doi.org/10.26165/JUELICH-DATA/YWB5P1, 2022.

Vereecken, L., Carlsson, P. T. M., Novelli, A., Bernard, F., Brown, S. S., Cho, C., Crowley, J. N., Fuchs, H., Mellouki, W., Reimer, D., Shenolikar, J., Tillmann, R., Zhou, L., Kiendler-Scharr, A., and Wahner, A.: Theoretical and experimental study of peroxy and alkoxy

radicals in the NO$_3$-initiated oxidation of isoprene, Phys. Chem. Chem. Phys., 23, 5496–5515, https://doi.org/10.1039/D0CP06267G, 2021.

1045   Wagner, N. L., Dubé, W. P., Washenfelder, R. A., Young, C. J., Pollack, I. B., Ryerson, T. B., and Brown, S. S.: Diode laser-based cavity ring-down instrument for NO$_3$, N$_2$O$_5$, NO, NO$_2$ and O$_3$ from aircraft, Atmos. Meas. Tech., 4, 1227–1240, https://doi.org/10.5194/amt-4-1227-2011, 2011.

Wennberg, P. O., Bates, K. H., Crounse, J. D., Dodson, L. G., McVay, R. C., Mertens, L. A., Nguyen, T. B., Praske, E., Schwantes, R. H., Smarte, M. D., St Clair, J. M., Teng, A. P., Zhang, X., and Seinfeld, J. H.: Gas-Phase reactions of isoprene and its major oxidation products,

1050   Chem. Rev., 118, 3337–3390, https://doi.org/10.1021/acs.chemrev.7b00439, 2018.

Whalley, L. K., Edwards, P. M., Furneaux, K. L., Goddard, A., Ingham, T., Evans, M. J., Stone, D., Hopkins, J. R., Jones, C. E., Karunaharan, A., Lee, J. D., Lewis, A. C., Monks, P. S., Moller, S. J., and Heard, D. E.: Quantifying the magnitude of a missing hydroxyl radical source in a tropical rainforest, Atmos. Chem. Phys., 11, 7223–7233, https://doi.org/10.5194/acp-11-7223-2011, 2011.

Wolfe, G. M., Crounse, J. D., Parrish, J. D., St. Clair, J. M., Beaver, M. R., Paulot, F., Yoon, T., Wennberg, P. O., and Keutsch, F. N.:

1055   Photolysis, OH reactivity and ozone reactivity of a proxy for isoprene-derived hydroperoxyenals, Phys. Chem. Chem. Phys., 14, 7276–7286, https://doi.org/10.1039/C2CP40388A, 2012.

Wu, R., Vereecken, L., Tsiligiannis, E., Kang, S., Albrecht, S. R., Hantschke, L., Zhao, D., Novelli, A., Fuchs, H., Tillmann, R., Hohaus, T., Carlsson, P. T. M., Shenolikar, J., Bernard, F., Crowley, J. N., Fry, J. L., Brownwood, B., Thornton, J. A., Brown, S. S., Kiendler-Scharr, A., Wahner, A., Hallquist, M., and Mentel, T. F.: Molecular composition and volatility of multi-generation products formed from isoprene

1060   oxidation by nitrate radical, Atmos. Chem. Phys., 21, 10 799–10 824, https://doi.org/10.5194/acp-21-10799-2021, 2021.

Xiong, F., McAvey, K. M., Pratt, K. A., Groff, C. J., Hostetler, M. A., Lipton, M. A., Starn, T. K., Seeley, J. V., Bertman, S. B., Teng, A. P., Crounse, J. D., Nguyen, T. B., Wennberg, P. O., Misztal, P. K., Goldstein, A. H., Guenther, A. B., Koss, A. R., Olson, K. F., de Gouw, J. A., Baumann, K., Edgerton, E. S., Feiner, P. A., Zhang, L., Miller, D. O., Brune, W. H., and Shepson, P. B.: Observation of isoprene hydroxynitrates in the southeastern United States and implications for the fate of NO$_X$, Atmos. Chem. Phys., 15, 11 257–11 272,

1065   https://doi.org/10.5194/acp-15-11257-2015, 2015.

Xiong, F., Borca, C. H., Slipchenko, L. V., and Shepson, P. B.: Photochemical degradation of isoprene-derived 4,1-nitrooxy enal, Atmos. Chem. Phys., 16, 5595–5610, https://doi.org/10.5194/acp-16-5595-2016, 2016.

Appendix A: Additional Figures and Tables

Table A1. Organic products expected to be produced from the oxidation of isoprene in this work and the ion mass (m/z) at which they are detected by the mass spectrometry instruments, which measured in the experiments. Evaluation of the ion mass signals of the Br^--CIMS instrument includes both major isotopes of Br. Only the chemical structure of one isomer of the same compound is shown.

Organic product	Sum formula	molecular weight	ion mass (m/z) VOCUS PTR-MS	ion mass (m/z) Br^--CIMS	ion mass (m/z) I^--CIMS
	$C_5H_8O_3$	116	117	195 / 197	370
	$C_4H_5NO_4$	131	132	210 / 212	385
	$C_5H_8O_4$	132	133	211 / 213	386
	$C_5H_7NO_4$	145	146	224 / 226	399
	$C_5H_9NO_4$	147	148	226 / 228	401
	$C_5H_7NO_5$	161	162	240 / 242	415
	$C_5H_9NO_4$	163	164	242 / 244	417
	$C_5H_9NO_5$	179	180	258 / 260	433
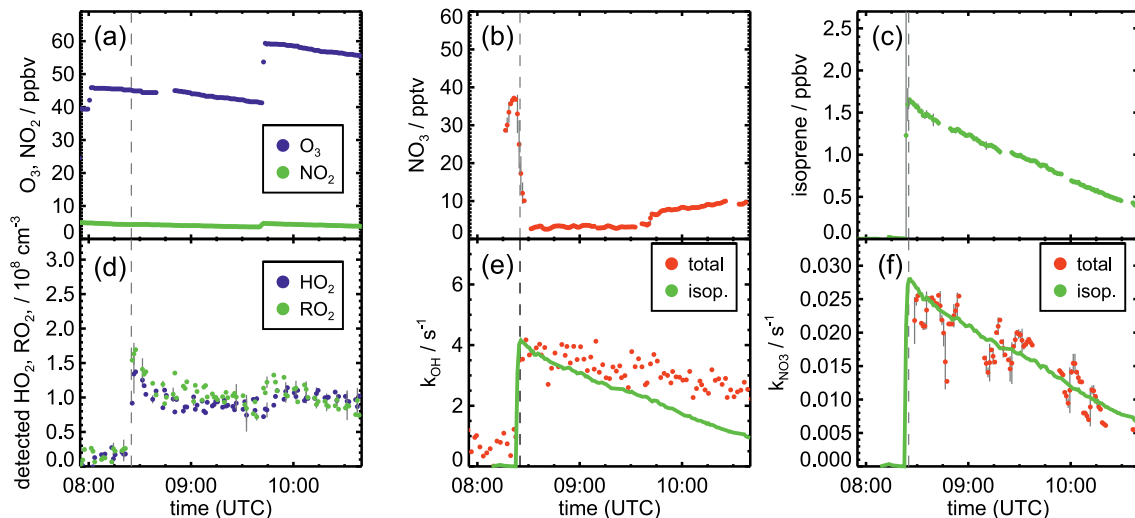
Figure A1. Measurements of radical and trace gas concentrations and OH and NO_3 reactivity in the experiment on 10 August 2018 (Experiment #2) investigating the oxidation of isoprene by NO_3. NO_3 reactivity does not include reactivity from organic radicals and NO_2. OH and NO_3 reactivity from isoprene is calculated from measured isoprene concentrations and reaction rate constants recommended in literature (Mellouki et al., 2021). Observed RO_2 radicals only include a fraction of the total RO_2 because the LIF instrument cannot detect all RO_2 radicals formed in the reaction of isoprene with NO_3 (Vereecken et al., 2021).
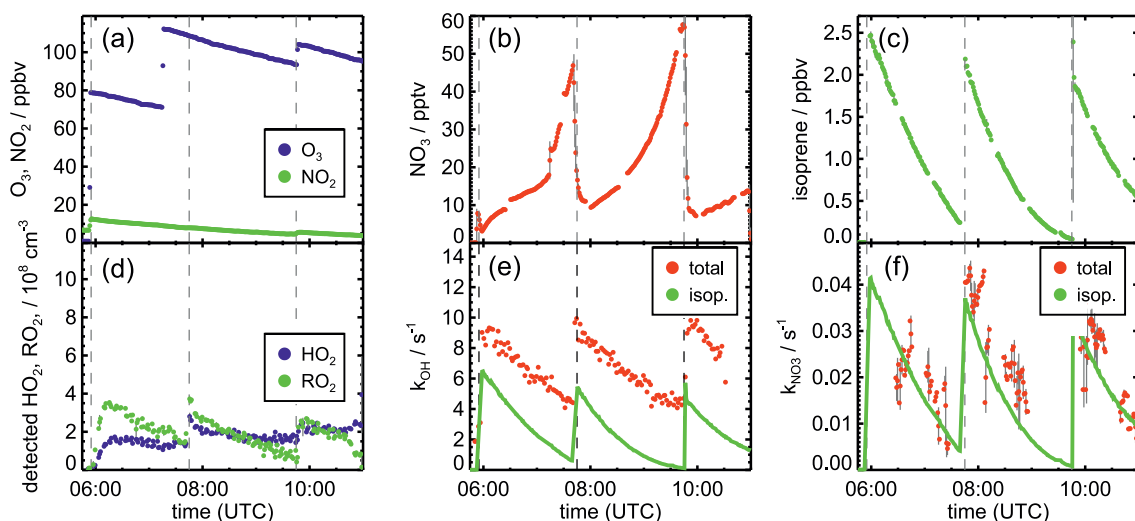
Figure A2. Measurements of radical and trace gas concentrations and OH and NO_3 reactivity in the experiment on 12 August 2018 (Experiment #3) investigating the oxidation of isoprene by NO_3. NO_3 reactivity does not include reactivity from organic radicals and NO_2. OH and NO_3 reactivity from isoprene is calculated from measured isoprene concentrations and reaction rate constants recommended in literature (Mellouki et al., 2021). Observed RO_2 radicals only include a fraction of the total RO_2 because the LIF instrument cannot detect all RO_2 radicals formed in the reaction of isoprene with NO_3 (Vereecken et al., 2021).
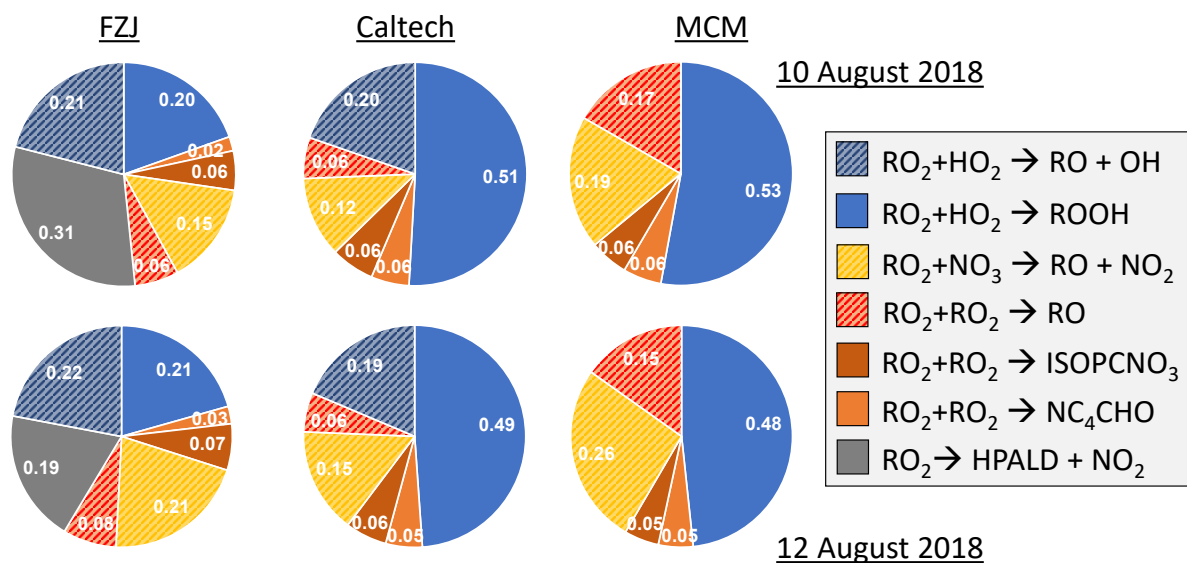
Figure A3. Relative distribution of loss rates of nitrate RO_2 for the experiment on 10 August 2018 (Experiment #2) and on 12 August 2018 (Experiment #3). The total RO_2 loss rate was 0.005 and $0.008\,\text{s}^{-1}$ in the experiment on 10 August 2018 (Experiment #2) and 12 August 2018 (Experiment #3), respectively. Calculations of the loss rates of RO_2 radicals in bimolecular reactions make use of measured HO_2 and NO_3 concentrations. Total RO_2 concentrations and concentrations of speciated nitrate RO_2 were taken from model calculations applying either the FZJ-NO3, Caltech or MCM mechanism. The chemical mechanisms differ with respect to the number of nitrate RO_2 isomers that are considered, the type of RO_2 loss reactions and products of loss reactions (Fig. 3 and 6). Therefore, the distibutions of nitrate RO_2 radicals and RO_2 concentrations differ between the model runs.
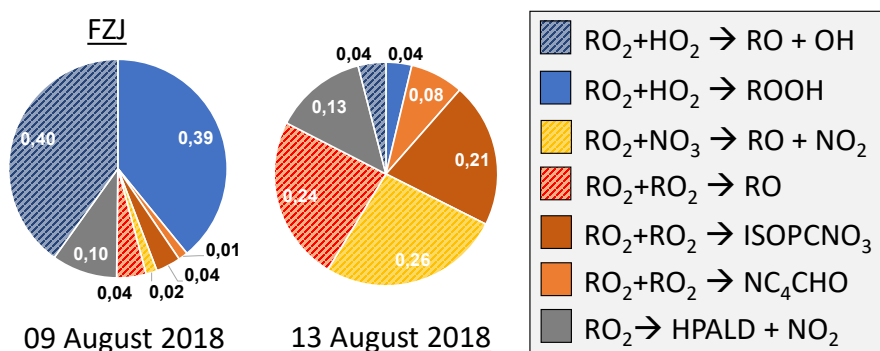
Figure A4. Relative distribution of loss rates of nitrate RO_2 for the experiment on 13 August 2018 (Experiment #3) if the FZJ-NO3 mechanism is applied and HO_2 is not constrained to measured values. Total RO_2 concentrations and concentrations of speciated nitrate RO_2 were taken from model calculations.
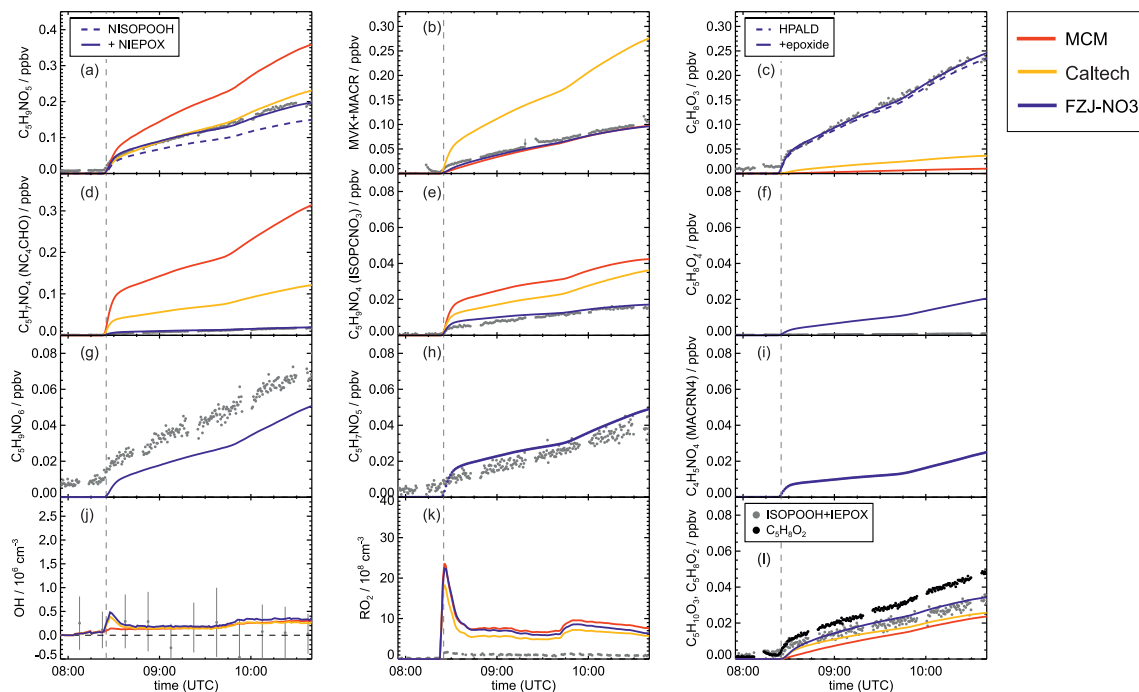
Figure A5. Comparison of results from model calculations applying the different isoprene NO_3 chemistry mechanisms for the experiment on 10 August 2018 (Experiment #2). MVK, MACR, NISOPOOH, $ISOPCNO_3$ and NC_4CHO are produced from all mechanisms, whereas the other compounds are only produced from either 1,6-H-shift reactions or ring-closure reactions of nitrate alkoxy radicals, which are only implemented in the FZJ-NO3 mechanism. Grey and black dots are measured values. Measured organic peroxy radical concentrations only include part of the total RO_2 because the LIF instrument cannot detect a fraction of nitrate RO_2 (Vereecken et al., 2021). Organic products were detected by the VOCUS PTR-MS instrument, which was only calibrated for MVK and MACR. All other traces are scaled to match best the results from the FZJ-NO3 mechanism.

Figure A6. Comparison of results from model calculations applying the different isoprene NO_3 chemistry mechanisms for the experiment on 12 August 2018 (Experiment #3). MVK, MACR, NISOPOOH, $ISOPCNO_3$ and NC_4CHO are produced from all mechanisms, whereas the other compounds are only produced from either 1,6-H-shift reactions or ring-closure reactions of nitrate alkoxy radicals, which are only implemented in the FZJ-NO3 mechanism. Grey and black dots are measured values. Measured organic peroxy radical concentrations only include part of the total RO_2 because the LIF instrument cannot detect a fraction of nitrate RO_2 (Vereecken et al., 2021). Organic products were detected by the VOCUS PTR-MS instrument, which was only calibrated for MVK and MACR. All other traces are scaled to match best the results from the FZJ-NO3 mechanism.

Figure A7. Comparison of reported signals from three mass spectrometer instruments applying different ionization methods (VOCUS PTR-MS, Br^--CIMS, I^--CIMS measuring organic products in the experiment on 09 August 2018 (Experiment #1). All signals are scaled to match best the concentrations resulting from model calculations applying the FZJ-NO3 chemical mechanism.
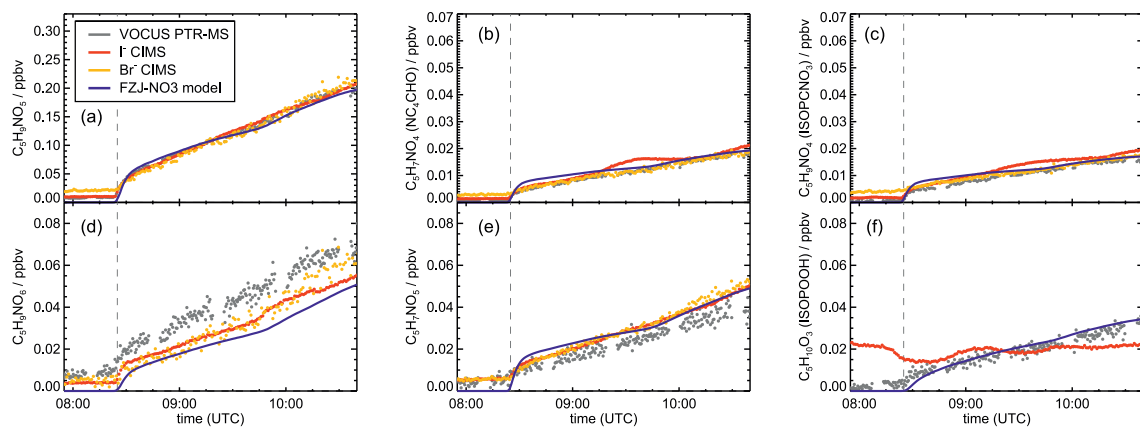
Figure A8. Comparison of reported signals from three mass spectrometer instruments applying different ionization methods (VOCUS PTR-MS, Br^--CIMS, I^--CIMS measuring organic products in the experiment on 10 August 2018 (Experiment #2). All signals are scaled to match best the concentrations resulting from model calculations applying the FZJ-NO3 chemical mechanism.
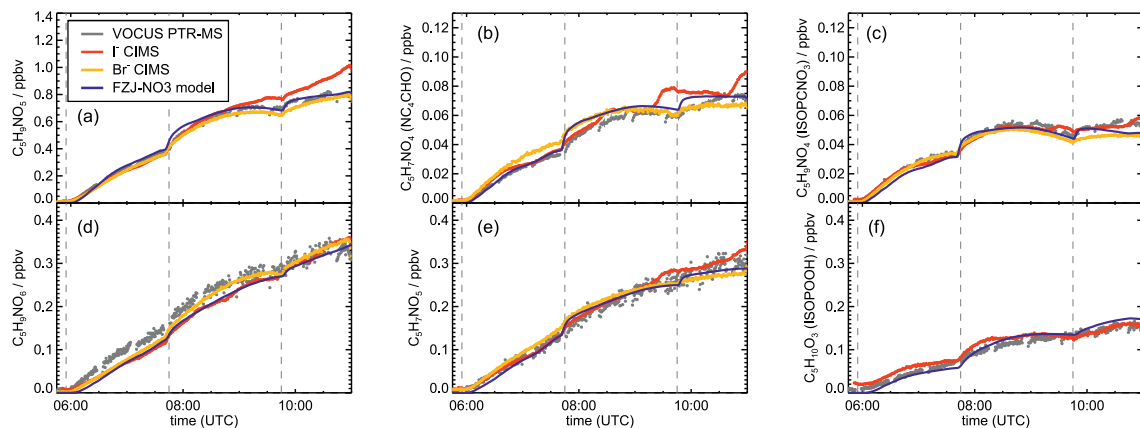
Figure A9. Comparison of reported signals from three mass spectrometer instruments applying different ionization methods (VOCUS PTR-MS, Br^--CIMS, I^--CIMS measuring organic products in the experiment on 12 August 2018 (Experiment #3). All signals are scaled to match best the concentrations resulting from model calculations applying the FZJ-NO3 chemical mechanism.
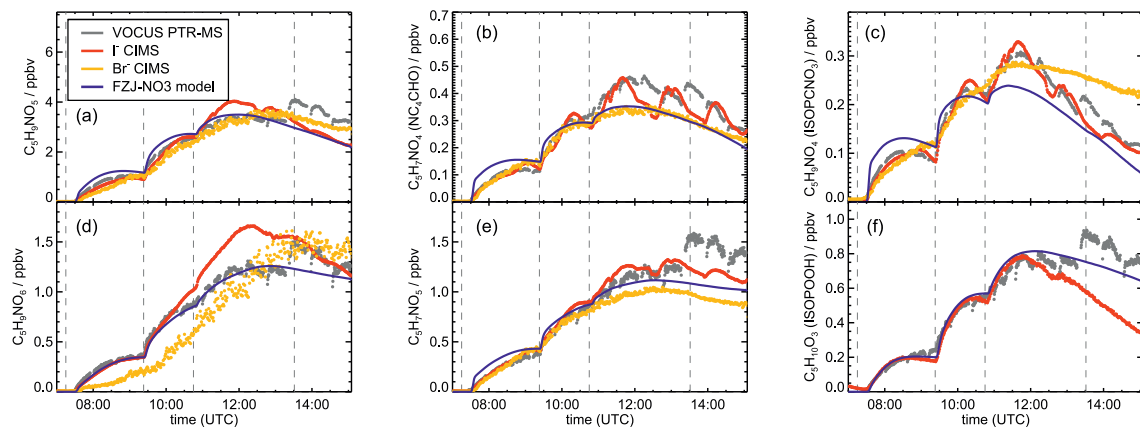
Figure A10. Comparison of reported signals from three mass spectrometer instruments applying different ionization methods (VOCUS PTR-MS, Br^--CIMS, I^--CIMS measuring organic products in the experiment on 13 August 2018 (Experiment #4). All signals are scaled to match best the concentrations resulting from model calculations applying the FZJ-NO3 chemical mechanism.
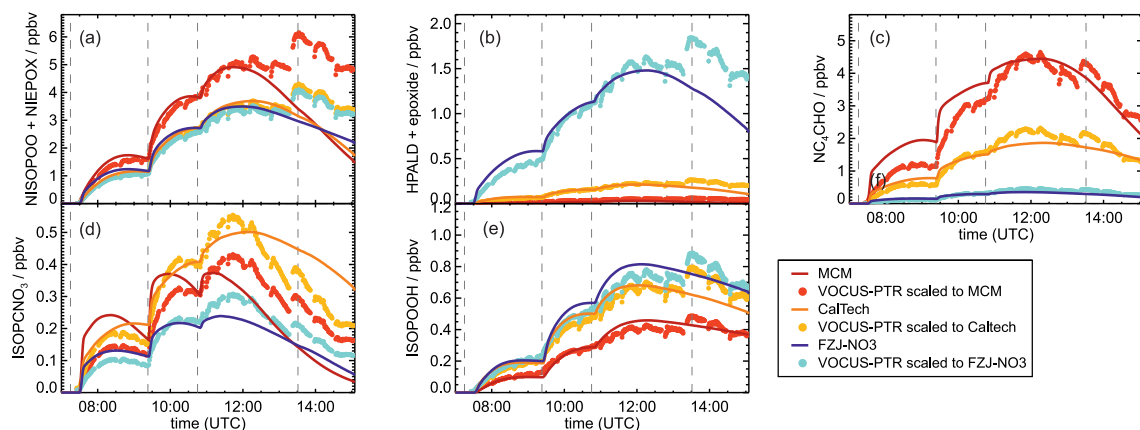
Figure A11. Ion mass signal of the VOCUS PTR-MS instrument scaled to the model results from the MCM, Caltech and FZJ-NO3 models in the experiment on 13 August 2018 (Experiment #4). Only species for which the instrument was not calibrated and which are produced in all models are shown.
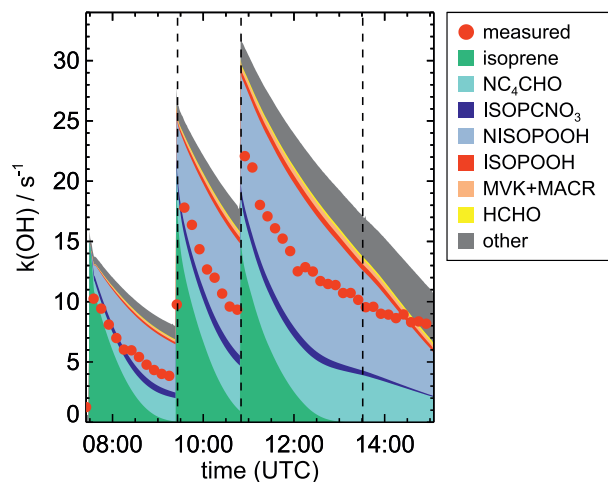
Figure A12. Comparison of measured OH reactivity from organic compounds and OH reactivity calculated from concentrations of organic compounds modelled applying the MCM chemical mechanism. Up to 10 % of the reactivity from hydroperoxide compounds (NISOPOOH, ISOPOOH) is invisible for the LP-LIF instrument, because these species produce partly OH in their reaction with OH. The exact OH yield is uncertain. 100 % yield is assumed in the MCM. OH reactivity from organic compounds is derived by subtracting the reactivity from NO_2 and O_3 calculated from measured concentrations from the measured total OH reactivity. "Other" compounds include a high number of organic compounds that are produced in the reaction of isoprene with OH, O_3 and NO_3 and for which loss by the reaction with OH is implemented in the MCM mechanism.